IKAROS levels are associated with antigen escape in CD19- and CD22-targeted therapies for B-cell malignancies

Pablo Domizi [1] ✉, Jolanda Sarno [1,2,3], Astraea Jager[1], Milton Merchant[1], Kaithlen Zen B. Pacheco[4], Sean A. Yamada-Hunter [4], Maria Caterina Rotiroti[5], Yuxuan Liu[1], Reema Baskar [6], Warren D. Reynolds[4], Brian J. Sworder[7], Bita Sahaf[4], Sean C. Bendall [6], Charles G. Mulligan [8], Ash A. Alizadeh [7,9,10], Allison B. Leahy[11,12], Regina M. Myers[11,12], Bonnie Yates[13], Hao-Wei Wang [14], Nirali N. Shah [13], Robbie G. Majzner [5], Crystal L. Mackall [4], Stephan A. Grupp [11,12], David M. Barrett[15], Elena Sotillo [4] & Kara L. Davis [1,4] ✉

Antigen escape relapse is a major challenge in targeted immunotherapies, including CD19- and CD22-directed chimeric antigen receptor (CAR) T-cell for B-cell acute lymphoblastic leukemia (B-ALL). To identify tumor-intrinsic factors driving antigen loss, we perform single-cell analyses on 61 B-ALL patient samples treated with CAR T cells. Here we show that low levels of IKAROS in pro-B-like B-ALL cells before CAR T treatment correlate with antigen escape. IKAROS^{low} B-ALL cells undergo epigenetic and transcriptional changes that diminish B-cell identity, making them resemble progenitor cells. This shift leads to reduced CD19 and CD22 surface expression. We demonstrate that CD19 and CD22 expression is IKAROS dose-dependent and reversible. Furthermore, IKAROS^{low} cells exhibit higher resistance to CD19- and CD22-targeted therapies. These findings establish a role for IKAROS as a regulator of antigens targeted by widely used immunotherapies and in the risk of antigen escape relapse, identifying it as a potential prognostic target.

B-cell acute lymphoblastic leukemia (B-ALL) is the most common childhood cancer, accounting for 25% of cancer diagnoses in children and adolescents up to 19 years of age[1]. Approximately 15% of children and young adults diagnosed with ALL will relapse, and 50% of children who relapse will die, making relapsed B-ALL the second leading cause of cancer-related death for children in the U.S[1]. Adult B-ALL has a dismal prognosis, with only 40% of patients alive 5 years from diagnosis[2]. CD19-directed CAR T (CART19) cells are now standard therapy for children and adults with relapsed or refractory B-ALL, achieving remission rates of 70 – 90%[3,4]. Unfortunately, around 50% of

[1]Department of Pediatrics, Hematology, Oncology, Stem Cell Transplant and Regenerative Medicine, Stanford University, Stanford, CA, USA. [2]Tettamanti Center, Fondazione IRCCS San Gerardo dei Tintori, Monza, Italy. [3]School of Medicine and Surgery, University of Milano-Bicocca, 20126 Milan, Italy. [4]Center for Cancer Cell Therapy, Stanford Cancer Institute, Stanford University School of Medicine, Stanford, CA, USA. [5]Department of Pediatric Oncology, Dana-Farber Cancer Institute, Boston, MA, USA. [6]Department of Pathology, Stanford University, Stanford, CA, USA. [7]Division of Oncology, Department of Medicine, Stanford University School of Medicine, Stanford, CA, USA. [8]Department of Pathology, St. Jude Children's Research Hospital, Memphis, TN, USA. [9]Institute for Stem Cell Biology and Regenerative Medicine, Stanford University, Stanford, CA, USA. [10]Stanford Cancer Institute, Stanford University, Stanford, CA, USA. [11]Division of Oncology, Children's Hospital of Philadelphia, Philadelphia, PA, USA. [12]Department of Pediatrics, Perelman School of Medicine, University of Pennsylvania, Philadelphia, PA, USA. [13]Pediatric Oncology Branch, Center for Cancer Research, National Cancer Institute, National Institutes of Health, Bethesda, MD, USA. [14]Laboratory of Pathology, National Cancer Institute, National Institutes of Health, Bethesda, MD, USA. [15]Kite Pharma, Santa Monica, CA, USA. ✉e-mail: domizi@stanford.edu; kardavis@stanford.edu

initial responders will eventually relapse, many with CD19 loss[5,6]. Similarly, CD19^{neg} relapses have been reported in patients treated with blinatumomab, an anti-CD3/CD19 bispecific T cell engager[7,8]. For patients suffering CD19^{neg} relapse, CD22-targeted therapies, either inotuzumab ozogomycin or CD22-directed CAR T (CART22) cells, have emerged as a salvage option[9]. However, CD22 downregulation has limited durable remissions[10]. Several mechanisms of CD19 loss have been reported, including truncated CD19 mutations[11], disruption of CD19 trafficking to the cell surface[12,13], CD19 mRNA mis-splicing[14,15], and lineage switch[16]; fewer studies have focused on the mechanisms behind CD22 downregulation, but alternative splicing has also been reported[17]. In several studies, CD19 loss was accompanied by CD22 downregulation[18–22]. Recovery of CD19 and CD22 expression has been reported after relief of immune pressure[17,18,23,24].

To discover cell-intrinsic factors associated with antigen loss, we analyzed 39 pre- and post-CART19 patient-derived xenografts (PDXs) from 25 patients using mass cytometry (CyTOF) and single-cell RNA and antibody tag sequencing (CITE-seq). In pre-CART19 samples, we identified CD19^{pos} pro-B-like tumor cells with low expression of the transcription factor IKAROS to be associated with CD19^{neg} relapse. We determined that IKAROS regulates CD19 expression in B-ALL, large B cell lymphoma (LBCL), and chronic lymphoblastic lymphoma (CLL) models. IKAROS^{low} cells demonstrate a wholesale change in chromatin and transcriptional state, shifting their identity away from B cells and moving towards myeloid and progenitor states. This loss of B cell identity manifests with decreased CD19 and CD22 surface expression. Consistent with this, we confirmed low IKAROS levels are also associated with CD22^{low} relapse in an independent cohort of 11 r/r B-ALL patients treated with CART22. IKAROS-mediated decrease in CD19 and CD22 surface expression confers a survival advantage for IKAROS[low] B-ALL cells against CD19- and CD22-targeted therapies. Together, we describe a role for IKAROS in immunotherapy target regulation and implicate pre-existing IKAROS^{low} cells at risk of antigen loss under the pressure of CD19- or CD22-targeted therapies in patients with B-cell malignancies.

Results

CD19 loss is accompanied by loss of B cell features

To identify tumor-intrinsic factors associated with CD19^{neg} relapse following CAR T therapy, we profiled 35 patient-derived xenograft (PDX) samples from pediatric and adult leukemia patients treated with 19.BBz CAR T cells using CyTOF (Fig. 1A, Supplementary Tables 1 and 2). This cohort includes pre-CART19 PDX samples from patients who achieved durable complete remission (CR; $n = 6$), underwent CD19^{neg} ($n = 11$) or CD19^{pos} ($n = 4$) relapse, or were non-responders ($n = 4$). We also analyzed paired post-CART19 relapse PDX samples from 14 of these patients, including those with CD19^{neg} relapse ($n = 8$), CD19^{pos} relapse ($n = 2$), or non-response ($n = 4$). Evaluation of CD19 expression in pre-CART19 PDX samples did not show differences across the clinical groups (Fig. 1B).

We applied our B-cell developmental classifier to compare cell types across patients[25]. Consistent with our prior findings in de novo B-ALL[25], most leukemic cells were classified within the pre-pro-B to pre-BI transitional populations, particularly as pro-BII-like B-ALL cells (Fig. 1C–D). Interestingly, after CD19 loss, a significant fraction of B-ALL cells were classified as early-non-BI (Fig. 1D). Early-non-BI cells are progenitor cells that do not express CD19 or other pan B-cell markers (Supplementary Fig. 1B). Enrichment in the early-non-BI population after CART19 was not observed in patients with CD19^{pos} relapse ($n = 2$) or refractory patients ($n = 4$; Supplementary Fig. 2A–B). This enrichment was not observed when comparing isogenic CD19 wild-type (WT) or knockout (KO) B-ALL cell lines (Supplementary Fig. 2C), suggesting that the sole loss of CD19 expression does not alter the developmental profile of B-ALL cells. Instead, in patients, CD19 loss is accompanied by the loss of additional B-cell features.

### Low levels of IKAROS in pro-B-like tumor cells are associated with CD19^{neg} relapse

Since pro-BII-like B-ALL cells were the most abundant across all patient groups (Fig. 1D), we compared protein expression in pro-BII-like cells from patients who achieved durable CR or underwent CD19^{neg} relapse. While CD19 and PAX5 expression did not differ between pre-treatment groups, pro-BII-like cells from patients who would experience CD19^{neg} relapse had lower expression of the B-lineage transcription factor IKAROS (Fig. 1E). This difference in IKAROS level was specific to pro-BII-like cells. It was not observed in the bulk leukemia cells or any other population (Supplementary Fig. 2D).

To further explore the differences between patients who achieved durable CR and those who underwent CD19^{neg} relapse, we performed CITE-seq on cells from healthy BM ($n = 1$), pre-CART19 samples from patients who achieved CR ($n = 3$), and paired pre- and post-CD19^{neg} relapse samples ($n = 3$) (Fig. 1F, Supplementary Table 3). We defined 18 cell populations in the healthy BM based on gene and protein expression profiles (Fig. 1G, Supplementary Fig. 3A, Supplementary Data 1). Then, we projected each B-ALL cell onto the healthy BM space (Fig. 1H) and assigned its closest healthy population. Most B-ALL cells were associated with healthy hematopoietic multipotent progenitor cells (HSC/MPP, cluster 9) or pro-B cells (cluster 6) (Fig. 1I). Although bulk samples and HSC/MPP-like B-ALL cells showed no differences in gene expression across clinical outcomes (Supplementary Fig. 3B–C), pre-CART19 pro-B-like B-ALL cells from patients with durable CR or CD19^{neg} relapse exhibited distinct gene signatures (Supplementary Fig. 3D). In particular, *IKZF1* expression was significantly lower in pre-CART19 CD19^{neg} relapse pro-B-like B-ALL cells (Fig. 1J, Supplementary Data 2). This was not true in bulk samples or HSC/MPP-like cells (Supplementary Fig. 3e). There were no differences in *CD19* mRNA, CD19 protein, or *PAX5* mRNA levels in pre-CART19 pro-B-like B-ALL cells (Supplementary Fig. 3F), consistent with our findings at the protein level (Fig. 1E). Pre-CART19 *IKZF1*^{low} pro-B-like B-ALL cells from patients who suffered CD19^{neg} relapse were enriched for an HSC/MPP gene expression signature, indicating these cells had less B-cell identity before CART19 administration (Fig. 1K). These features, low levels of IKZF1 expression and enrichment in HSC/MPP gene expression signature, were conserved after CD19 loss (Fig. 1J–K).

IKAROS modulates CD19 splicing and CD19 surface expression

To investigate the impact of IKAROS on CD19 surface expression, we targeted IKAROS in B-ALL cell lines using two separate short hairpin RNA (shRNA) sequences (KD1 and KD2, Fig. 2A), or lenalidomide, a cereblon inhibitor that targets IKAROS for degradation[26] (Fig. 2B), or a combination of both methods (KD1 with or without 10 μM lenalidomide, Fig. 2C). These experiments confirmed that decreased IKAROS levels reduced CD19 surface expression. Furthermore, we confirmed the relationship between IKAROS and CD19 surface expression in LBCL (Supplementary Fig. 4A–C) and CLL (Supplementary Fig. 4D) models, suggesting that IKAROS modulation of CD19 surface expression is consistent across B cell malignancies.

To understand how IKAROS modulates CD19 surface expression, we analyzed isogenic IKAROS wild-type (WT) and knockdown (KD) B-ALL cell lines using ATAC-seq and RNA-seq (Supplementary Fig. 4E). Transcriptomic data showed similar *CD19* mRNA levels in IKAROS WT and KD cells (Fig. 2D). Chromatin accessibility at the *CD19* promoter and gene locus also showed no changes (Fig. 2E, Supplementary Fig. 5A). However, gene set enrichment analysis (GSEA) demonstrated enrichment of genes associated with RNA splicing in IKAROS WT cells, suggesting potential alterations in splicing events in IKAROS KD cells (Fig. 2F). *CD19* mis-splicing has been reported to influence CD19 expression[14,15]. In particular, *CD19* intron 2 retention, which encodes a truncated CD19 protein, has been reported in healthy BM, pre-CART19
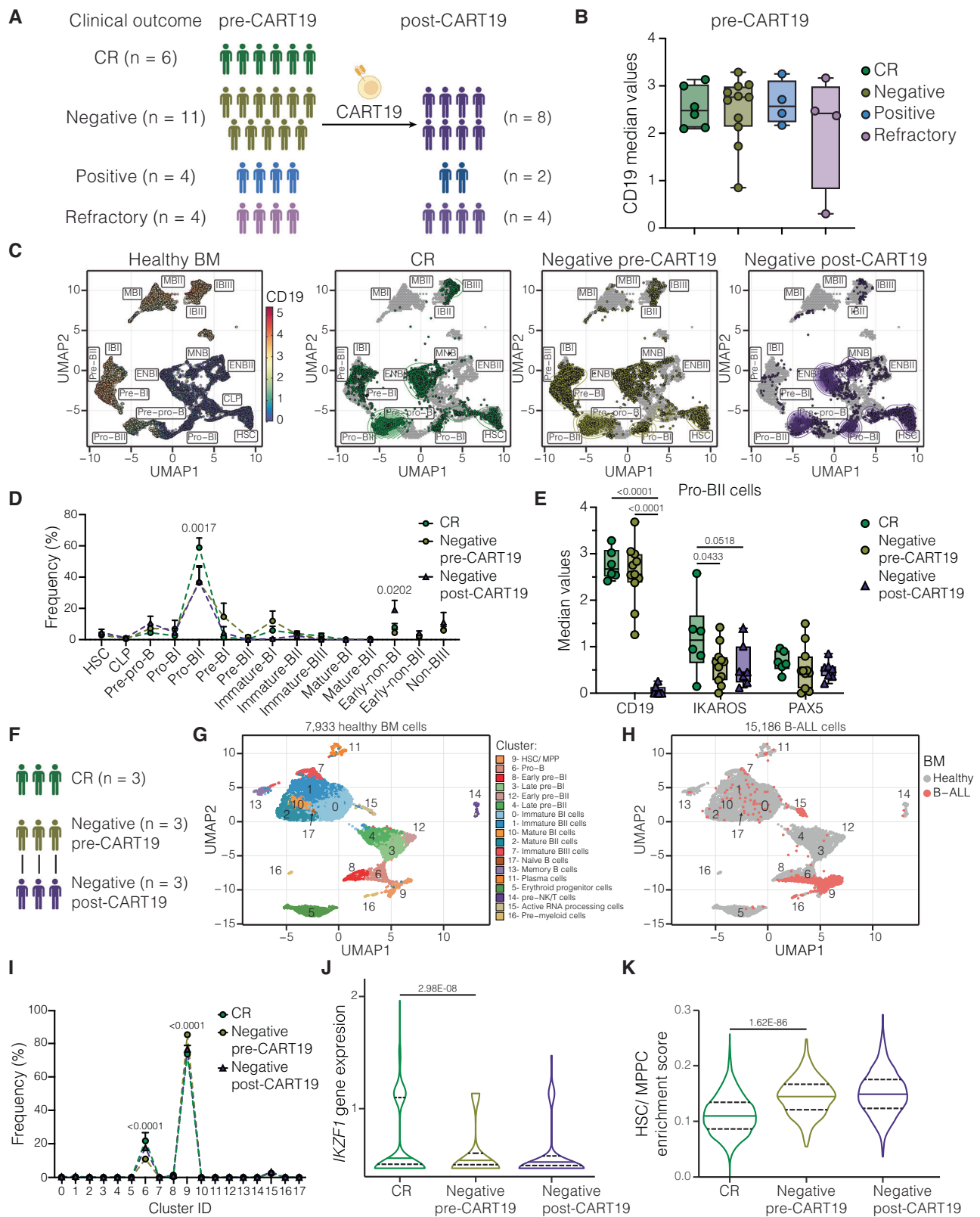
leukemic blasts, and associated with CD19^{neg} relapse[15,27,28]. While baseline retention of *CD19* intron 2 was already high in B-ALL cell lines (79.6%), IKAROS KD B-ALL cells showed a trend toward higher retention (86.1%; Supplementary Fig. 6D). Interestingly, a different splicing event, *CD19* intron 10 retention, was significantly higher in IKAROS KD cells (Fig. 2G). We observed more *CD19* intron 10 retention in CD19^{neg} relapsed samples from pediatric B-ALL patients treated with 19.BBz

CAR T cells[11,14] (*n* = 11), adult B-ALL patients treated with blinatumomab[13] (*n* = 2), and adult LBCL patients treated with 19.28z CAR T cells[29,30] (*n* = 6) (Fig. 2H, Supplementary Fig. 6E). *CD19* intron 10 retention was confirmed to occur in 282 diagnosis or relapse B-ALL patient samples from the TARGET dataset (Supplementary Fig. 6A). Of note, the annotated *CD19* transcript retaining intron 10 also retains intron 2 (ENST00000565089, Supplementary Fig. 6B). Analysis of

Fig. 1 | CD19 loss is associated with loss of B cell identity. A CART19 cohort of PDX samples analyzed by CyTOF. Created in BioRender[81]. **B** Median CD19 expression in CR ($n = 6$), Negative ($n = 11$), Positive ($n = 4$), and Refractory ($n = 4$) pre-CART19 samples. **C** UMAP based on developmental classifier protein expressions in Lin-/ B+ fraction of healthy BM (left) and projection of tumor cells from pre-CART19 patients that achieved durable CR ($n = 6$), suffered CD19^{neg} relapse ($n = 11$), and post-CD19 loss ($n = 8$), respectively. IBI Immature-BI, IBII Immature-BII, IBIII Immature-BIII, MBI Mature-BI, MBII Mature-BII, ENBI Early-non-BI, ENBII Early-non-BII, NBIII Non-BIII.. **D** Developmental classification of samples in (**C**). The pro-BII population is significantly more abundant in the CR group (CR vs. Negative pre-CART19 p-value: 0.0005; CR vs. Negative post-CART19 p-value: 0.0017), while early-non-BI is significantly more abundant between the pre- and post-CD19^{neg} relapse groups (p-value = 0.0202). **E** Median protein expression of CD19, IKAROS, and PAX5 in pro-BII-like tumor cells in CR ($n = 6$), Negative pre-CART19 ($n = 11$), and Negative post-CART19 ($n = 7$) samples. **F** Cohort of pre-and post-CART19 B-ALL samples analyzed by single-cell CITE-seq. **G** UMAP based on most variables genes in Lin-/ B+ fraction of healthy BM. Space occupied by healthy clusters is depicted. **H** Projection of B-ALL cells from 9 samples onto healthy BM-defined UMAP space. **I** B-ALL cells

from CR ($n = 3$), Negative pre-CART19 ($n = 3$), and Negative post-CART19 ($n = 3$) samples were associated with their closest healthy cluster based on k-nearest neighbor assignment. Cluster 6 is significantly less abundant in the Negative pre-CART19 group (Negative pre-CART19 vs. CR p-value < 0.0001; Negative pre-CART19 vs. Negative post-CART19 < 0.0001), while cluster 9 is significantly more abundant in the Negative pre-CART19 group (Negative pre-CART19 vs. CR p-value < 0.0001; Negative pre-CART19 vs. Negative post-CART19 < 0.0001). **J–K** *IKZF1* gene expression (**J**) and single-cell enrichment score for HSC/MPP gene signature (**K**) in pro-B-like B-ALL cells (cluster 6). N represents individual patient samples. Patient samples analyzed by mass cytometry or single-cell CITE-seq were not performed in replicates. Boxplots in (**B**) and (**E**) extend from the 25th to the 75th percentiles, with a line in the middle representing the median and whiskers extending from the minimum to the maximum values. Curves in (**D**) and (**I**) show mean ± SEM. Violin plots in (**J**) and (**K**) show the median (solid line) and 25th and 75th quantile (dash lines). The statistical tests used were one-way ANOVA followed by Tukey's multiple comparisons tests (**B**); two-way ANOVA followed by Tukey's multiple comparisons tests (**D**), (**E**), and (**I**); and two-sided Wilcoxon rank sum test followed by Bonferroni's multiple comparisons test in (**J**) and (**K**).

direct long-read RNA-seq data from one B-ALL patient (SRR14326969), confirmed that *CD19* intron 10 was co-retained with intron 2 (Supplementary Fig. 6C). *CD19* intron 2 retention was higher in CD19^{neg} relapsed pediatric and adult B-ALL, and LBCL patients (Supplementary Fig. 6E). To assess the impact of *CD19* intron 10 on CD19 surface expression, we introduced different CD19 isoforms into CD19 KO B-ALL models (Supplementary Fig. 6F). As expected, the presence of *CD19* intron 2 completely abolished CD19 surface expression, whereas inclusion of *CD19* intron 10 had no effect (Supplementary Fig. 6G), suggesting that intron 10 retention may serve as a proxy for intron 2 retention.

IKAROS is required to sustain B-cell identity and CD22 surface expression

ATAC-seq analysis identified 1250 and 4037 peaks significantly more accessible in IKAROS WT and KD cells, respectively (Supplementary Data 3), consistent with IKAROS' role as a transcriptional repressor[31]. The transcription factor binding sites in these differentially accessible peaks differed between IKAROS WT and KD cells (Supplementary Fig. 7A), indicating altered gene expression programs in IKAROS KD cells. Transcriptomic analysis confirmed differential expression of several transcription factors between IKAROS WT and KD cells (Supplementary Fig. 7B, Supplementary Data 4). IKAROS KD cells showed 168 genes with both more accessible promoters and higher expression, forming a network characterized by non-B lineage genes (red nodes in Supplementary Fig. 7C), suggesting a loss of B cell identity. Indeed, while the gene expression profile and chromatin landscape of IKAROS WT cells are consistent with pro-B cell identity (Fig. 2J, Supplementary Fig. 4G), IKAROS KD cells acquired a profile more characteristic of HSC/MPP cells (Fig. 2I, J).

Given the re-wiring of transcriptional networks in IKAROS KD cells, we investigated the expression of other B-cell proteins. IKAROS KD cells showed reduced *CD22* mRNA (Fig. 2K) and CD22 surface expression (Fig. 2L). IKAROS KD also demonstrated increased expression of alternatively spliced *CD22* isoforms that retain intron 2 or skip exon 12 (Supplementary Fig. 6H). Clinical trials have targeted CD22 in patients who relapse after CD19-targeted therapies[10]. We analyzed 22 paired patient samples collected before CART22 administration or after CD22^{low} relapse to assess the clinical implications of IKAROS and CD22 interaction. Lower IKAROS levels were found in pro-BII-like B-ALL cells following CD22^{low} relapse (Fig. 2M, Supplementary Table 1). These results suggest that IKAROS modulates CD19 and CD22 surface expression, and patients with IKAROS^{low} tumor cells might be at higher risk for antigen-loss relapse following both CD19- and CD22-targeted therapy.

IKAROS regulates CD19 and CD22 surface expression in a dose-dependent and reversible manner

To fine-tune IKAROS levels without the toxicities associated with shRNA infection and lenalidomide treatment, we generated IKAROS-regulatable models by overexpressing a codon-optimized version of IKAROS fused to a degron tag[32] and knocked out the endogenous *IKZF1* gene. In this system, in the absence of asunaprevir, a hepatitis C virus nonstructural protein 3 protease inhibitor, cells express high levels of IKAROS as the degron tag is removed. However, in the presence of asunaprevir, IKAROS is rapidly targeted for degradation. We generated seven models (IKAROS-degron KO1 – KO7) where IKAROS levels can be titrated using different concentrations of asunaprevir (Fig. 3A). CD19 and CD22 surface levels decreased in an IKAROS dose-dependent manner (Fig. 3B, C). We selected IKAROS-degron KO1 and KO2 models for further studies because they express the highest and lowest baseline CD19 surface expression, respectively. Upon asunaprevir withdrawal, IKAROS, CD19, and CD22 levels were restored (Fig. 3D–F), demonstrating reversible regulation of CD19 and CD22 surface expression by IKAROS.

CyTOF analysis of IKAROS-degron models treated with asunaprevir for 3, 7, or 22 days showed downregulation of CD19 and CD22 surface expression along with mature B-cell (CD24, CD38, CD72) and B-cell differentiation (PU.1) proteins in IKAROS[low] conditions. Conversely, proteins in progenitor (CD10, CD43), myeloid (CD58, CD63, RUNX1), and antigen-presenting (HLA-DR) cells were upregulated (Fig. 3G). These phenotypic changes promote a shift of IKAROS^{low} cells toward more progenitor and immature B-cell states (Fig. 3H–I), confirming previous observations of the transcriptional and chromatin landscapes.

IKAROS alterations are associated with relapse in de novo B-ALL[33]. The most common IKAROS alteration is the deletion of the four DNA-binding domains, resulting in the dominant negative IK6 isoform[34]. To assess whether patients expressing the IK6 isoform—who are more likely to experience chemotherapy failure and subsequently receive CD19- or CD22-targeted therapies—are at higher risk for antigen escape relapse, we generated IK6-degron models (Supplementary Fig. 8A). Surface CD19 and CD22 molecules were similar among IKAROS-degron and IK6-degron models (Supplementary Fig. 8B). Interestingly, decreasing IK6 expression with asunaprevir treatment did not modify CD19 or CD22 surface levels in IK6-degron models (Fig. 3J–L). CyTOF protein profiling revealed that asunaprevir treatment did not alter the expression of CD38, CD58, CD72, or RUNX1, while the effects on CD24, PU.1, and HLA-DR expression were attenuated (Supplementary Fig. 8C). CD45 was the only protein that showed a distinct response to asunaprevir treatment, being upregulated in IK6-degron cells (Supplementary Fig. 8c). Similarly, IK6-degron models did not exhibit a
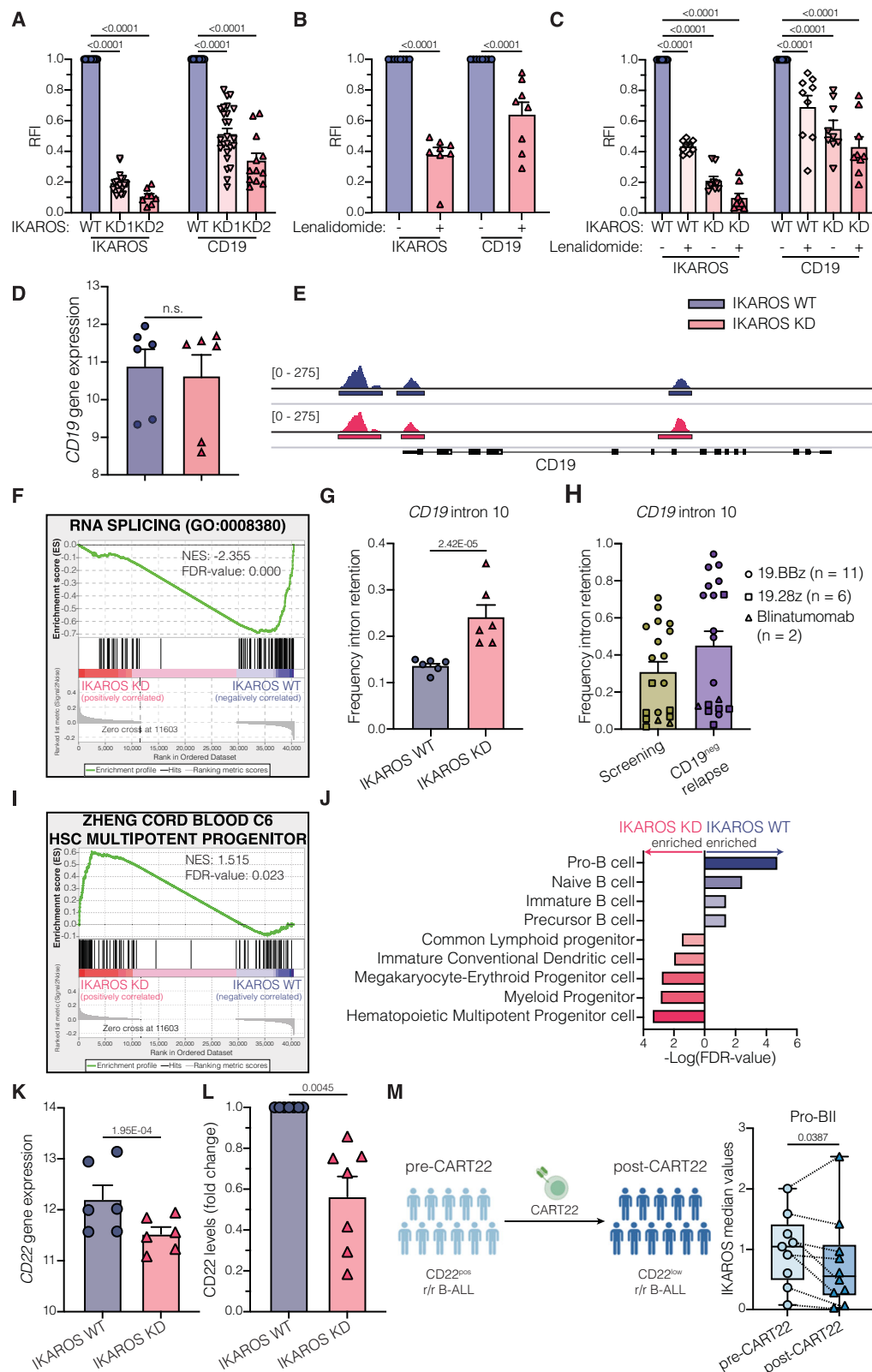
developmental shift following asunaprevir treatment (Supplementary Fig. 8D). Consistent with the results of our model, in primary patient data, there are no differences in *CD19* or *CD22* gene or protein expression between patients with *IKZF1* deletions and those with other B-ALL subtypes (Supplementary Fig. 8E, F). These results suggest that patients with *IKZF1* deletions are not more susceptible to CD19 or CD22 downregulation, and in the context of CD19- and CD22-targeted

therapies, the response is instead related to wild-type IKAROS dose and requires the DNA binding domains.

Low levels of IKAROS confer resistance to CD19- and CD22-targeted therapies

Since antigen density is crucial for CAR T cell efficacy[35], we investigated whether IKAROS^{low} cells have an advantage against CD19- and

Fig. 2 | IKAROS regulates CD19 and CD22 surface expression. A–C Relative IKAROS and CD19 median levels in B-ALL cell lines (697, NALM6, NALM16, NALM20, REH, RS4;11, SUP-B15) transduced with lentivirus expressing scrambled or short hairpin RNA (shRNA) against *IKZF1* (**A**; n from left to right: 20, 20, 8, 25, 25, 12), treated with DMSO or 10 μM lenalidomide (**B**; *n* = 8), or combining shRNA knockdown with or without lenalidomide treatment (**C**, *n* = 9). Proteins were measured by flow cytometry and normalized to scrambled transduced (**A**), DMSO-treated (**B**), or scrambled transduced and DMSO-treated (**C**) cells. RFI = relative fluorescence intensity. N represents independent biological replicates. **D** *CD19* variance-stabilized transformed (vst) counts in IKAROS WT or KD B-ALL cells. **E** Accessibility profile of *CD19* promoter and gene from one representative IKAROS WT and KD B-ALL cell line pair. Other cell lines and their biological replicates can be found in Supplementary Fig. 5A. **F** Gene set enrichment analysis (GSEA) results for RNA splicing (GO: 0008380) gene signature in IKAROS WT and KD B-ALL cells. **G, H** Frequency of intron 10 retention in *CD19* mRNA in IKAROS WT or KD B-ALL cells (**G**) or pediatric B-ALL patients treated with 19.BBz CAR T cells[11,14] (*n* = 11), adult B-ALL patients treated with blinatumomab[13] (*n* = 2), and adult LBCL patients treated with 19.28z CAR T cells[29,30] (*n* = 6) (**H**). **I** GSEA results

for Zheng Cord Blood C6 HSC/MPP gene signature[80] in IKAROS WT and KD B-ALL cells. **J** Cell type enrichment analysis of genes with differentially accessible promotors in IKAROS WT or IKAROS KD B-ALL cells. **K** *CD22* vst counts in IKAROS WT or KD B-ALL cells. **L** Relative CD22 median levels in isogenic IKAROS WT or KD B-ALL cells (*n* = 7; independent biological replicates). Values were measured by flow cytometry or CyTOF and normalized to IKAROS WT condition. **M** Paired pre-CART22 and post-CD22^{low} relapse cohort of leukemic patient samples analyzed by CyTOF. IKAROS median levels in pro-BII-like tumor cells. **N** represents individual patient samples. Schematic representation of the patient cohort created in BioRender[81]. RNA-seq and ATAC-seq experiments (**D–G, I–K**) were performed in 3 cell lines (NALM6, REH, and SUP-B15) with two biological replicates per cell line. Bar plots in (**A–D**), (**G, H**), and (**K, L**) show mean ± SEM. Boxplots in (**M**) extend from the 25th to the 75th percentiles, with a line in the middle representing the median and whiskers extending from the minimum to the maximum values. Statistical tests used were two-way ANOVA followed by Šidák's multiple comparisons test (**A–C**); DESeq's Wald test followed by BH correction (**D**) and (**K**); multivariate analysis of transcript splicing (rMATS) followed by FDR correction (**G**); and two-sided paired t-test (**L**) and (**M**). Not significant (n.s.), *P* > 0.05.

CD22-targeted therapies. First, we confirmed that low IKAROS levels significantly reduced the number of CD19 and CD22 molecules on the B-ALL cell surface (Fig. 4A–C). Then, we co-cultured asunaprevir- or vehicle-treated IKAROS-degron cells with mock, blinatumomab, 19.BBz, 19.28z, 22.BBz, and dual 19/22.BBz CAR T cells. At three different effector-to-target ratios, IKAROS^{low} cells were more resilient to CD19- and CD22-targeted therapies (Fig. 4D–H, Supplementary Fig. 9), with more pronounced resistance at lower effector-to-target ratios.

To determine if the advantage of IKAROS^{low} cells against these therapies was due to reduced antigen expression and to rule out the effect of other IKAROS-regulated genes (Supplementary Fig. 4F, Supplementary Data 4), we developed a model whereby CD19 levels were unaffected by IKAROS. We knocked out the endogenous *CD19* gene in our IKAROS-degron models and reintroduced ectopic expression of wild-type CD19. In these models, named CD19KO-FL, asunaprevir treatment reduced IKAROS levels without decreasing CD19 surface expression (Supplementary Fig. 10A), while the changes in other proteins persisted (Supplementary Fig. 10B). As expected, asunaprevir treatment did not provide any advantage against CD19-targeted therapies, even at low E:T ratios (Supplementary Fig. 10C–E). Thus, decreased CD19 and CD22 surface expression due to low IKAROS levels reduces the efficacy of CD19- and CD22-targeted therapies and B-ALL cell killing, demonstrating that IKAROS^{low} cells have a survival advantage in the face of these therapies (Fig. 5).

Discussion

Antigen loss after targeted immunotherapies, including blinatumomab, CD19- or CD22-directed CAR T cells, remains a significant clinical challenge for patients with r/r B-cell malignancies. There is no standard of care for patients experiencing a CD19^{neg} relapse, and outcomes are poor[9,36]. Often, CD22 is the next antigen targeted, as it is expressed in the majority of B-ALL[9,10,37,38]. Here, we found that the transcription factor IKAROS modulates CD19 and CD22 surface expression in a dose-dependent and reversible manner. IKAROS is a transcription factor crucial in B cell lineage specification and commitment and is a known B-ALL tumor suppressor[39]. In B-ALL, genetic alterations affecting the IKAROS gene, *IKZF1*, are associated with poor response to front-line therapy and are a factor in relapse risk stratification[33]. However, a role for IKAROS in the failure of CD19- and CD22-targeted therapies has not been described.
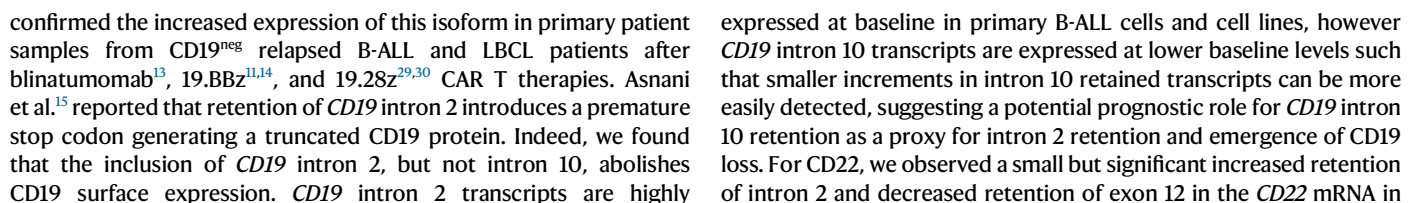
Two non-mutually exclusive models explain the source of CD19^{neg} tumor cells. First, the immune-enrichment model posits that rare pre-existing CD19^{neg} tumor cells are selected while antigen-positive cells are eradicated[40,41]. A single-center study of 166 pediatric and young adult r/r B-ALL cases treated with tisagenlecleucel found that the presence of CD19[neg/dim] tumor cells prior to therapy did not predict

nonresponse or recurrence after CART19 therapy[42]. Second, the immune-pressure adaptive model suggests that some CD19^{pos} tumor cells possess intrinsic properties that favor losing CD19 to CD19 targeting[13]. Our data support the latter model. Using single-cell approaches in clinically annotated samples, we found that, prior to CART19 therapy, CD19^{pos} pro-B-like tumor cells with low levels of IKAROS were associated with CD19 loss and CD19^{neg} relapse. Notably, IKAROS levels differed only in pro-B-like cells, not in other sub-populations, highlighting the power of our single-cell approach.

IKAROS[low] pro-B-like tumor cells are enriched for an HSC/ MPP gene signature, demonstrating loss of B-cell commitment. CD19 loss has been associated with increased expression of stem/progenitor markers, such as CD34 and CD123, suggesting de-differentiation to a developmentally earlier state[43]. IKAROS KD or regulatable models demonstrated that B-ALL cells acquire the HSC/MPP signature through modulation of IKAROS. Low levels of IKAROS resulted in the modulation of B-cell phenotype with a gain of stem/progenitor and myeloid proteins while B-lineage proteins declined. These include targets of immune therapies in B-ALL (CD22[44], CD38[45], and CD72[46]), suggesting more potential for phenotypic plasticity and lineage infidelity. Wholesale modulation of B-ALL cell state and phenotype aligns with previous observations in cell line models and patients, where CD19 loss was accompanied by CD22 downregulation[18–22] and loss of both antigens is reversible[17,23].

Although not addressed in our study, lineage switch relapses occur after CD19-directed therapy[16]. Several studies suggest that the acquisition of myeloid features at relapse originates from CD19^{pos} B-ALL cells through reprogramming or selection of clones with HSPC features[47–50]. Our data suggest that IKAROS^{low} cells have increased plasticity and potential for lineage infidelity and thus may be ripe to support lineage switch. It is likely, however, that only those with the right conditions (genomic background, cytokine signaling) will be able to overcome the barrier to differentiate towards the myeloid compartment, consistent with the model presented by Jacoby et al.[49].

Identification of several molecular mechanisms underlying antigen loss has emerged with the usage of targeted therapies. CD19 loss has been associated with truncating mutations of the *CD19* gene[11], mutations in genes involved in CD19 membrane trafficking[12,13], and *CD19* mRNA alternative splicing[14,15]. CD22 downregulation, which is less understood than CD19 loss, has been reported through alterations in transcription and splicing[17]. Alternative splicing is a complex and rapid way to reversibly fine-tune the expression of specific genes. Further, there is no evidence to suggest that these potential mechanisms are mutually exclusive, meaning mutations in CD19 and mis-splicing events may co-occur. We found that low levels of IKAROS result in increased *CD19* mRNA with co-retention of introns 2 and 10 and

confirmed the increased expression of this isoform in primary patient samples from CD19^{neg} relapsed B-ALL and LBCL patients after blinatumomab[13], 19.BBz[11,14], and 19.28z[29,30] CAR T therapies. Asnani et al.[15] reported that retention of *CD19* intron 2 introduces a premature stop codon generating a truncated CD19 protein. Indeed, we found that the inclusion of *CD19* intron 2, but not intron 10, abolishes CD19 surface expression. *CD19* intron 2 transcripts are highly expressed at baseline in primary B-ALL cells and cell lines, however *CD19* intron 10 transcripts are expressed at lower baseline levels such that smaller increments in intron 10 retained transcripts can be more easily detected, suggesting a potential prognostic role for *CD19* intron 10 retention as a proxy for intron 2 retention and emergence of CD19 loss. For CD22, we observed a small but significant increased retention of intron 2 and decreased retention of exon 12 in the *CD22* mRNA in

Fig. 3 | IKAROS regulates CD19 and CD22 surface expression in a dose-dependent and reversible manner. A–C Relative IKAROS (**A**, $n = 7$), CD19 (**B**, $n = 7$), and CD22 (**C**, $n = 2$) median levels in IKAROS-degron models treated with increasing doses of asunaprevir. Values were measured by flow cytometry and normalized to DMSO-treated ($0 \mu M$) condition. N represents independent clones. Dots represent the mean value from two technical replicates. RFI relative fluorescence intensity. **D–F** IKAROS-degron models were treated with $10 \mu M$ asunaprevir for 7 days. Afterward, asunaprevir was withdrawn, and cells were either treated with DMSO (ASU/DMSO) or maintained with $10 \mu M$ asunaprevir (ASU/ASU) for an additional 28 days. As a control, IKAROS-degron models were treated with DMSO for 35 days. Relative levels of IKAROS (**D**), CD19 (**E**), and CD22 (**F**) were measured at 9, 14, 21, and 28 days post-asunaprevir withdrawal by flow cytometry and normalized to DMSO-treated condition. The experiment was performed in duplicate using two independent clones ($n = 2$). RFI relative fluorescence intensity. **G** IKAROS-degron models were treated with DMSO (D0; $n = 6$; 2 independent clones in 3 independent experiments) or $10 \mu M$ asunaprevir for 3 ($n = 2$; 2 independent clones in 2 independent experiments), 7 ($n = 4$; 2 independent clones in 2 independent experiments), and 22 ($n = 2$ independent clones) days. The protein profile was measured by flow cytometry and CyTOF and normalized to the D0 condition. **H** Projection of IKAROS-degron models treated with DMSO (left) or $10 \mu M$ asunaprevir (right) for 7 days onto the UMAP representation of healthy B cell developmental populations based on developmental classifier protein expressions. **I** Developmental classification of samples in (**G**). The frequencies of Pro-BII and Pre-BI populations were statistically different (p-value < 0.001) in the D0 condition against D3, D7, and D22 conditions. **J, K** Relative IK6 (**A**, $n = 3$), CD19 (**B**, $n = 3$), and CD22 (**C**, $n = 3$) median levels in IK6-degron models treated with increasing doses of asunaprevir. Values were measured by flow cytometry and normalized to DMSO-treated ($0 \mu M$) condition. N represents independent clones. Dots represent the mean value from two technical replicates. RFI relative fluorescence intensity. Bar plots in (**A–F**) and (**J–L**) show mean ± SEM. Boxplots in (**G**) extend from the 25th to the 75th percentiles, with a line in the middle representing the median and whiskers extending from the minimum to the maximum values. Curves in (**I**) show mean ± SEM. Statistical tests used were paired one-way ANOVA followed by Dunnett's multiple comparisons test (**A–C**) and (**J–L**); and two-way ANOVA followed by Dunnett's multiple comparisons test (**D–G**) and (**I**).

IKAROS KD models. The *CD22* intron 2 retained isoform results in a truncated CD22 protein, similar to previously reported *CD22* exon 2 skipped isoforms[17]. *CD22* exon 12 skipped isoform has been associated with more aggressive leukemias through the loss of CD22 immunoreceptor tyrosine-based inhibitory motifs[51,52]. Our data suggests the use of alternative splicing as a rapid way to modulate phenotypes during lineage decisions that support plasticity in leukemia, which requires further study.

In addition to differences in *CD19* and *CD22* mRNA splicing in IKAROS KD models, we found further distinctions in how IKAROS modulates CD19 versus CD22 surface expression. While there were no differences in *CD19* mRNA levels or promotor accessibility in IKAROS KD cells, *CD22* mRNA levels were significantly lower, with changes in the accessibility to two peaks in *CD22* intronic regions. Moreover, the kinetics for CD22 and CD19 surface expression recovery in the regulatable IKAROS model were different. These results suggest that IKAROS modulates CD19 and CD22 surface expression through different mechanisms, which will be the subject of future studies. Despite these distinctions, we show that IKAROS DNA binding domains are required to modulate CD19 and CD22 surface expression. *IKZF1* alterations occur in 25 to 80% of B-ALL cases, with *IKZF1* partial or complete deletions as the main alterations[34]. In our cohort, *IKZF1* deletions were only reported in two patients, and both were refractory to CART19 (Supplementary Table 1). The presence of *IKZF1* deletions did not correlate with lower *CD19* or *CD22* mRNA or protein levels. Thus, our data suggest that patients with *IKZF1* deletions are not more prone to antigen escape relapse following CD19- or CD22-targeted immunotherapies.

High disease burden prior to treatment, non-response to blinatumomab, and emergence of minimal residual disease are clinical features associated with CD19^{neg} relapse[36,42,53–55]. Prior blinatumomab induces higher expression of alternative CD19 isoforms, decreases CD19 surface expression, and selects tumor cells more fit to survive CD19-directed immunotherapies[13,42,55]. In our CART19 cohort, 5 patients received prior CD19-targeted therapy (blinatumomab or CART19); 4 of them suffered CD19^{neg} relapse, while the other achieved a durable CR. High disease burden may increase the frequency of IKAROS^{low} tumor cells. Furthermore, when challenged with CD19- and CD22-targeted therapies, IKAROS^{low} tumor cells had the most survival advantage at lower effector-to-target ratios, conditions that resemble higher tumor burdens, and indicate a higher probability for IKAROS^{low} tumor cells to survive and enable antigen escape relapse.

FDA approval for early administration of blinatumomab in frontline therapy and inotuzumab after the first non-response or relapse increases the population at risk for antigen escape. Hematopoietic stem cell transplantation (HSCT) has been used as a consolidative therapy to avoid antigen escape relapse but still risks long-term complications and side effects[56]. Understanding the mechanisms of antigen loss and thereby identifying patients at risk for antigen escape relapse would change the treatment paradigm for these challenging patients. Our results provide insight into mechanisms of antigen modulation and lineage plasticity mediated by IKAROS dose and demonstrate a potential prognostic role for IKAROS in the early identification of patients at risk of antigen loss and identify IKAROS as a target to revert or subvert these relapses.

Methods

Bone marrow samples from patients and healthy donors
Healthy human bone marrow (BM) was purchased from AllCells, Alameda, CA, USA ($n = 6$; median age was 23 years (range, 21 – 32 years); 5 males and 1 female). De-identified patient-derived xenograft (PDX) samples were obtained from Children's Hospital of Philadelphia. thirty-nine samples were collected under informed consent from twenty-three patients enrolled in CHP959 (NCT01626495[57]; $n = 18$), 14BT022 (NCT02228096[58]; $n = 4$), and 16CT022 (NCT02906371[59]; $n = 1$) studies; and two adult patients treated compassionately: one patient with r/r B-ALL that underwent CD19^{pos} relapse after CART19 treatment (Patient ID: Pos1) and one patient with chronic lymphocytic leukemia/small lymphocytic lymphoma (CLL/SLL) with Richter's transformation that underwent CD19^{neg} relapse after CART19 therapy (Patient ID: Neg11). All patients in this cohort were treated with 19.BBz CAR T cells. Twenty-two de-identified primary patient samples were obtained from 11 patients who were consented and treated with 22.BBz CAR T cells on a phase I trial (NCT02315612[60]) at the National Cancer Institute. The Stanford University Institutional Review Boards approved the use of these samples. Clinical data for these samples are available in Supplementary Table 1.

Cell culture and CD19 knock out generation
NALM6 (CRL-3273), REH (CRL-8286), RS4;11 (CRL-1873), and SUP-B15 (CRL-1929) cell lines were purchased from ATCC (Manassas, VI, USA). 697 (ACC 42), CI (ACC 770), JVM-2 (ACC 12), MHH-CALL4 (ACC 337), NALM16 (ACC 680), NALM20 (ACC 681), and WA-OSEL (ACC 767) were purchased from DSMZ (Braunschweig, Germany). OCI-Ly1, OCI-Ly-7, and SUDHL6 were a gift from the Amengual lab[61]. 697, JVM-2, NALM6, NALM16, REH, RS4;11, SUDHL6, and WA-OSEL were cultured in RPMI-1640 medium supplemented with 10% fetal bovine serum (FBS). OCI-Ly1 and OCI-Ly-7 were cultured in IMDM medium supplemented with 10% FBS. CI, MHH-CALL4, NALM20, and SUP-B15 were cultured in IMDM or RPMI-1640 medium supplemented with 20% FBS. For all cell
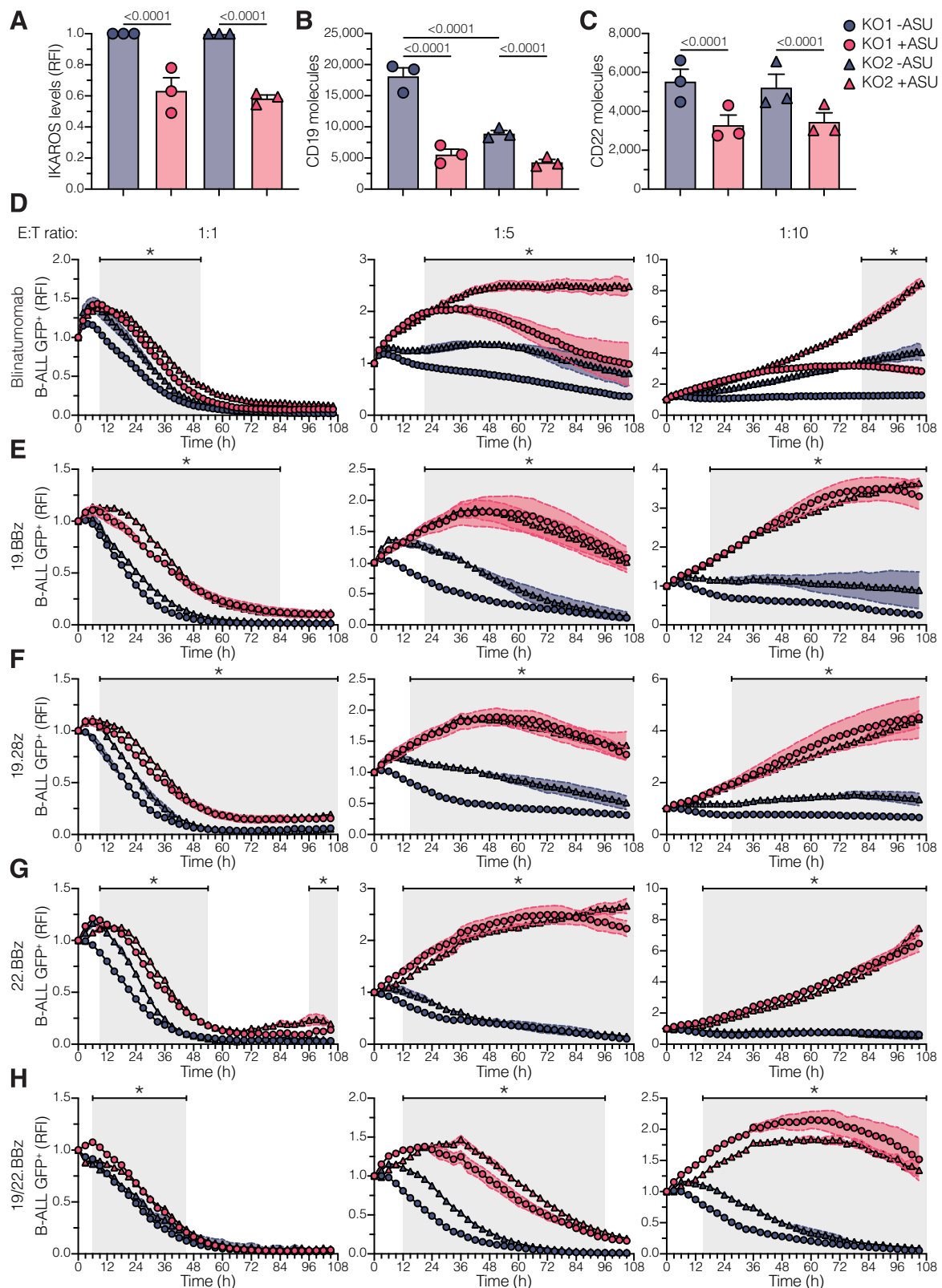
lines, the medium was additionally supplemented with 2 mM L-glutamine (Invitrogen) and 1x penicillin/streptomycin (Invitrogen), and cells were maintained at 37 °C and 5% CO_2.

To generate CD19 KO cell lines, we incubated 3.2 µg synthetic gRNA against the *CD19* gene (Synthego KO kit v2) with 6 µg purified Alt-R S.p. HiFi Cas9 Nuclease V3 (IDT) for 20 min at 37 °C. Guide sequences were as follows: 5′-UGCCAGGCCUUCUCAGAGGG-3′, 5′-UUUUUAAG AAGGGUUUAAGCG-3′, and 5′-CUUCAACGUCUCUCAACAGA-3′. This ribonucleoprotein complex was transfected into 1.5×10^5 MHH-CALL4, NALM6, REH, or SUP-B15 cells via electroporation using a 4D-Nucleofector system and AMAXA SF reagent with program CV-104 (Lonza). Seven days post-electroporation, cells were processed for CyTOF and CD19^{neg} (CD19 KO) cells were gated from CD19^{pos} (CD19 WT) cells.

Fig. 4 | Cells with low IKAROS expression are resistant to CD19- and CD22-targeted therapies. A Median IKAROS expression in IKAROS-degron models (KO1 and KO2) treated with DMSO (-ASU, $n = 3$) or 10 μM asunaprevir (+ASU, $n = 3$) for 7 days. Values were measured by flow cytometry and normalized to -ASU condition. N represents biological replicates from independent experiments. RFI relative fluorescence intensity. **B, C** CD19 (**B**) and CD22 (**C**) surface quantitation in IKAROS-degron models (KO1 and KO2) treated with DMSO (-ASU, $n = 3$) or 10 μM asunaprevir (+ASU, $n = 3$) for 7 days. N represents biological replicates from independent experiments. **D–H** IKAROS-degron models (KO1 and KO2) were treated with DMSO (-ASU) or 10 μM asunaprevir (+ASU) for 7 days. IKAROS-degron cells were washed out of DMSO or asunaprevir and co-cultured with blinatumomab-treated (**D**), 19.BBz (**E**), 19.28z (**F**), 22.BBz (**G**), and dual 19/22.BBz (**H**) CAR T cells at 1:1, 1:5, and 1:10 E:T ratio. B-ALL cell viability was measured at every 2 – 3 h interval via IncuCyte. GFP median values were normalized to 0 h condition. RFI relative fluorescence intensity. (*) denotes conditions in which both KO1 + ASU *vs.* KO1 -ASU and KO2 + ASU *vs.* KO2 -ASU comparisons were statically significant (*p*-values < 0.05). Please refer to the source data file for the exact *p*-value at each time point. Experiments in (**D–H**) were performed in triplicate with three different T-cell donors. Dots represent the mean value from two (**A–C**) or three (**D–H**) technical replicates. Bar plots in (**A–C**) show mean ± SEM. Curves in (**D–H**) show mean ± SEM. Statistical tests used were two-way ANOVA followed by Šidák's multiple comparisons test, with a single pooled variance (**A–C**); and two-way ANOVA followed by Šidák's multiple comparisons test (**D–H**).
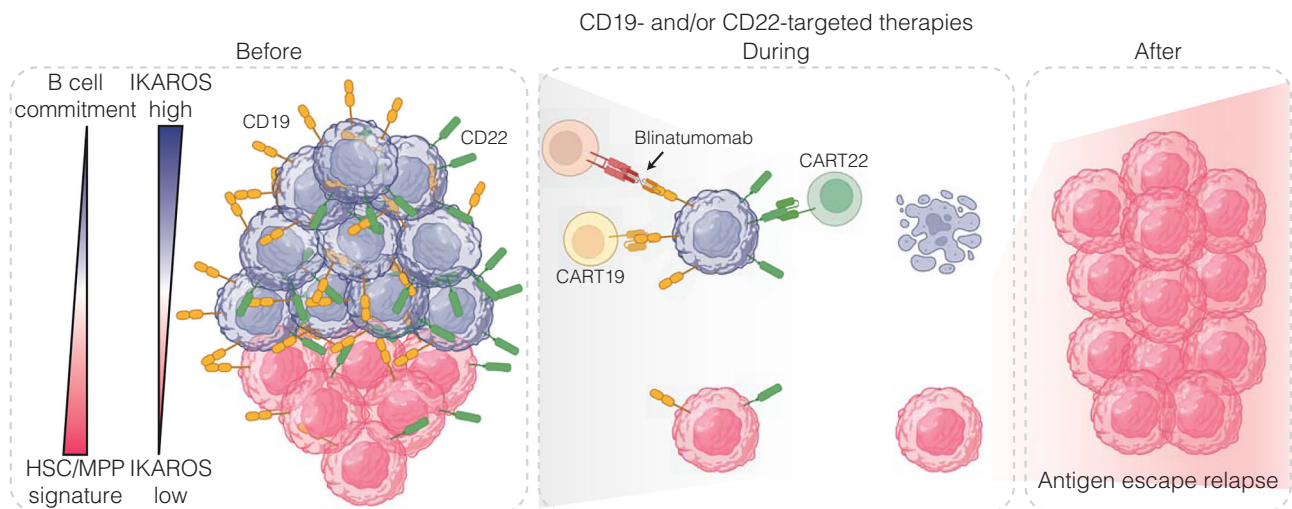
Fig. 5 | Proposed model of IKAROS-mediated antigen escape in the face of CD19- and CD22-targeted therapies. Before immunotherapy, IKAROS^{low} pro-B-like B-ALL cells possess chromatin and gene expression states poised for loss of B-cell identity while maintaining expression of CD19 and CD22. Under immune pressure, IKAROS^{high} cells maintain their antigen expression, making them more susceptible to T cell-mediated killing. Conversely, IKAROS^{low} cells are more likely to down-regulate their antigen expression, giving them a relative advantage to escape immunotherapies, resulting in antigen escape relapse. Created in BioRender[81].

Mass cytometry

Samples were processed as previously described[62]. For viable frozen healthy BM, leukemic primary, and PDX samples, cells were thawed in 90% RPMI medium (ThermoFisher Scientific) with 10% FCS, 20 U/ml sodium heparin (Sigma-Aldrich), 0.025 U/ml Benzonase (Sigma-Aldrich), 1x L-glutamine and 1x penicillin–streptomycin (Invitrogen) and rested at 37 °C for 30 min. For B-ALL cell lines, cells were resuspended in their corresponding culture media. For healthy BM, leukemic primary, and PDX samples, 1×10^6 cells were stained for viability with cisplatin as described[63]. Following viability staining, cells were fixed with 1.6% paraformaldehyde (PFA, Electron Microscopy Sciences) for 10 min at RT. Cells were barcoded using 20-plex palladium barcoding plates prepared in-house as described[64]. We included one healthy BM reference sample within each barcoding plate to control for batch effects. A total of 15 barcode plates were used in this study. Following barcoding, cells were pelleted and washed once with cell-staining medium (CSM; PBS with 0.5% BSA and 0.02% sodium azide) to remove residual PFA. Blocking was performed with Human TruStain FcX (BioLegend), following the manufacturer's instructions. Antibodies to surface proteins were added, yielding 800-μl final reaction volumes, and samples were incubated at RT and 300 g for 30 min (Supplementary Table 2). Cells were washed with CSM before permeabilization with methanol for 10 min at 4 °C. Cells were washed with CSM and stained with intracellular protein and phospho-specific antibodies in 800 μl for 30 min at RT and 300 g (Supplementary Table 2). Cells were washed once in CSM, then stained overnight with 1:5,000 191Ir/193Ir or 103Rh DNA intercalator (Standard Biotools) in PBS with 1.6% PFA at 4 °C. Cells were washed once with CSM, washed twice with double distilled water, filtered to remove aggregates, and resuspended in 139La/ 142Pr/ 159Tb/ 169Tm/ 175Lu normalization beads[65] immediately before analysis using a Helios mass cytometer (Standard Biotools). Throughout the analysis, cells were maintained at 4 ° C and introduced at a constant rate of 150–200 cells/s.

Processing of mass cytometry data

Data were normalized together using bead normalization[65] and files were debarcoded as described[64]. Single-cell protein expression data were extracted and analyzed using packages from the Comprehensive R Archive Network (CRAN) project (https://cran.r-project.org/) and Bioconductor (http://www.bioconductor.org). Raw data were transformed using the inverse hyperbolic sine (arcsinh) function with a cofactor of 5. The expression of proteins in each population of interest was determined by calculating the median level of expression after arcsinh transformation. For UMAP visualization, each population or sample was randomly subsampled to 1000 cells. Dimensionality reduction was performed using umap package (version 0.2.9.0) based on arcsinh values of selected markers.

Manual gating

Single cells were gated using Community Cytobank software (https://community.cytobank.org/) based on event length and 191Ir/193Ir or 103Rh DNA content (to avoid debris and doublets) as described[66]. For B-ALL cell lines, live B-ALL cells were gated based on cleaved poly(ADP-ribose) polymerase (cPARP) and ^{195}Pt or cleaved Caspase3 (cCaspase3)

content[63]. Downstream analyses were performed in this live B-ALL cell fraction. For healthy BM, leukemic primary, and PDX samples, following single-cell gating, live non-apoptotic cells were gated based on cleaved poly(ADP-ribose) polymerase (cPARP) and ^{195}Pt content[63]. In PDX samples, murine cells were excluded by gating on mouse CD45 (mCD45) protein. Platelets and erythrocytes were excluded by gating on CD61 and CD235a/b, respectively. The remaining fraction was gated to exclude T cells and myeloid cells based on CD3e, CD11b, CD16, and CD33 expression. After further exclusion of CD38^{high} plasma cells, the remaining fraction was defined as lineage-negative blasts (Lin − / B + ; see Supplementary Fig. 2A for gating). Further analyses were applied to Lin − / B+ fraction. For the primary samples in the CART22 cohort, we applied opt-SNE[67] to the Lin-/B+ fraction of each paired sample together with their corresponding healthy BM reference to gate blast cells, as was previously shown[68]. The following markers were used for opt-SNE: CD10, CD11b, CD16, CD179b, CD24, CD33, CD34, CD38, CD45, CD81, HLADR, intracellular immunoglobulin heavy chain (IgMi), surface immunoglobulin heavy chain (IgMs), Ki67, phosphorylated CREB, phosphorylated S6, and terminal deoxynucleotidyl transferase (TdT).

B-cell developmental classification

We used the single-cell developmental classifier previously reported[25]. Briefly, Lin − / B+ fraction from healthy human BM was gated into 15 developmental populations of normal B lymphopoiesis, mixed progenitors, and mature non-B cell fractions, as shown in Supplementary Fig. 1. The distribution of each population was based on the expression of 10 B cell developmental proteins that were used for manual gating: CD19, CD20, CD24, CD34, CD38, CD45, CD127, CD179b, IgMi, and TdT. Lin − / B+ cells from each leukemia sample or live B-ALL cells from cell lines samples were assigned to the most similar healthy fraction based on the shortest Mahalanobis distance among distances to all healthy developmental populations in these ten dimensions. A cell was designated 'unclassified' if none of the distances were below the classification threshold (Mahalanobis distance = 10, based on the number of dimensions).

Single cell RNA and antibody tag sequencing

Viably frozen healthy BM and PDX samples (Patient ID: CR2, CR4, CR6, Neg2, Neg5, Neg11) were thawed in 90% RPMI medium (ThermoFisher Scientific) with 10% FCS, 20 U/ml sodium heparin (Sigma-Aldrich), 0.025 U/ml Benzonase (Sigma-Aldrich), 1x L-glutamine and 1x penicillin–streptomycin (Invitrogen) and rested at 37 °C for 30 min. Then cells were filtered through cell strainer size 35 μm and centrifuged at 350 g for 5 min. Cells were resuspended in 1 ml of Stain Buffer (BD Biosciences) and blocking was performed with Human Fc Block (BD Biosciences) following the manufacturer's instructions. To enrich for Lin − / B+ fraction, samples were incubated with biotin-conjugated antibodies (Supplementary Table 3) for 30 min. Cells were washed with Stain Buffer and then incubated with BD Streptavidin Particles Plus (BD Biosciences) at the manufacturer's recommended concentration for 30 min at RT. Particle-labeled cells were placed in a magnetic holder for 6 min. The supernatant was transferred to a new tube and placed back in the magnetic holder for an additional round of depletion and supernatant recovery. Cells from the supernatant were then pelleted by centrifugation at 350 g for 5 min.

Lin-/ B+ fraction was resuspended in 180 μl of Stain Buffer supplemented with a mix of BD AbSeq oligo conjugated antibodies against CD19, CD20, CD24, CD34, CD38, CD45, CD127, and IgM (BD Biosciences, Supplementary Table 3). Then, each sample was labelled with the Human Single Cell Sample Multiplexing kit (BD Biosciences) and incubated at RT for 30 min. Cells were washed twice with Stain Buffer and resuspended in Sample Buffer (BD Biosciences). Cell number was counted with Countess II Cell Counter (Thermo Fisher Scientific). A total of 50,000 cells (12,500 cells per sample, up to 4 samples) were pooled together, and single cells were isolated in a BD Rhapsody

cartridge using BD Rhapsody Express Single-Cell Analysis System (BD Biosciences). We included one healthy BM reference sample within each cartridge to control for batch effects. A total of 3 cartridges were used in this study. For each cartridge, we followed the manufacturer's instructions to prepare whole transcriptomic, antibody tag, and sample tag libraries using the Whole Transcriptome Analysis (WTA) Amplification Kit (BD Biosciences). Libraries from the same cartridge were indexed with identical Illumina sequencing adapters. Final libraries were pooled together, sequencing on a NovaSeq 6000 sequencer (Illumina) at MedGenome (Foster City, CA, USA) with paired-end 100 base pair (bp) reads.

Processing of CITE-seq data

Fastq files were processed through the Rhapsody analysis pipeline (BD Biosciences) on the Seven Bridges platform (https://www.sevenbridges.com), following the manufacturer's recommendations. Reads were mapped to the hg38 reference genome using bowtie2. Final expression matrices contain recursive substation error correction (RSEC) adjusted molecule counts per cell in a CSV format. Molecule count tables were read into the R package Seurat (version 3.2). Out of 35,716 total cells, 2106 (5.9%) were multiplets, and 637 (1.8%) were undetermined events. The mean number of cells sequenced per sample was 2748. The mean number of genes detected per cell was 947, with a mean of 2670 reads/cell for the mRNA library and 1493 reads/cell for the antibody tag library. Cells with less than 500 expressed genes or 200 gene reads assigned and more than 50% of genes being mitochondrial genes were excluded for downstream analysis, removing 12,597 cells. We normalized transcriptomic data through variance stabilizing transformation with the removal of mitochondrial gene percentage as a potential confounding source of variation. Antibody tag data was normalized with a centered log-ratio transformation.

We performed the Wilcoxon rank sum test for differential expression analysis followed by Bonferroni correction. Genes and antibody tags expressed in at least 10% of cells from one of the conditions under comparison, had an absolute fold change higher or equal to 25%, and had adjusted *p*-value lower than 0.05 were called significant. Heatmaps were plotted using the ComplexHeatmap package (version 2.6.2), and the mean expression of each gene or antibody tag per population. To estimate the single-cell enrichment score for the HSC multipotent progenitor program, we used the function AddModuleScore from the Seurat package.

Projection of tumor cells onto healthy BM UMAP space

To define healthy BM populations and their UMAP space, we performed principal component (PC) analysis on 3000 most variable genes (MVG) across all healthy BM cells and antibody tag data. Based on the top 30 PCs, we performed UMAP embedding of healthy cells, as well as unsupervised clustering with the functions FindNeighbors and FindClusters from the Seurat package. We used the function FindMarkers to identify genes significantly *up*-regulated in each cluster against all the other clusters. Differentially expressed genes were analyzed with Enrichr[69] (https://maayanlab.cloud/Enrichr/) to define biological pathways associated with each cluster and assign their corresponding cell population.

To project tumor cells onto the healthy BM space, we predicted their top 30 PCs based on the PC analysis performed for the healthy BMs and the expression of 3000 MVG defined previously and antibody tag data. These predicted top 30 PCs were used to project and embed tumor cells onto healthy BM UMAP space. To associate each tumor cell with their closest healthy population, we used a k-nearest neighbors model (k-NN). Briefly, we performed 10-fold cross-validation to train a k-NN model to predict the cell population of healthy BM cells based on the top 30 PCs. For this model, the ten nearest neighbors were considered, and the decision was taken based on majority voting. Finally,

we defined the closest population to each tumor cell by applying this k-NN model to their predicted top 30 PCs.

Retrovirus and Lentivirus production

For retrovirus production, 293GP cells were used (graciously provided by Dr Garry Nolan). Briefly, 70% confluent 293GP on 10-cm poly-d-lysine coated plates were cotransfected with 9 µg of IKAROS-degron-P2A-mNeonGreen, IK6-degron-P2A-mNeonGreen, CD19WT-IRES-eGFP, CD19Int2-IRES-eGFP, CD19Int10-IRES-eGFP, CD19Int2-10-IRES-eGFP, 19.BBz, 19.28z, 22.BBz, or 19/22.BBz CAR encoding vectors and 4.5 µg RD114 envelope plasmid (graciously provided by Dr. Crystal Mackall) with lipofectamine 3000 (Invitrogen). Viral supernatants were collected 48 and 72 h post-transfection, centrifuged to separate cell debris from the viral supernatant, and frozen at −80 °C for future use.

For third-generation, self-inactivating lentivirus production, 4 – 5 × 10^6 293 T cells (graciously provided by Dr. Crystal Mackall) were plated on a 10-cm dish for 24 h before transfection. On the day of transfection, a mixture of 1.5 µg pMD2.G envelope plasmid (Addgene #12259), 2.25 µg psPAX2 packing plasmid (Addgene #12260), and 3.75 µg vector plasmid were cotransfected with TurboFect (Thermo Fisher). For the current study, we used the following vector plasmids: pLKO-RFP-shCntrl (Addgene #69040), pLKO-RFP-IKZF1-sh2 (Addgene #69041), pLKO-RFP-IKZF1-sh3 (Addgene #69042), SMARTvector Inducible Non-targeting PGK-TurboRFP (VSC11656, Horizon Discovery Biosciences), and SMARTvector Inducible Human IKZF1 PGK-TurboRFP shRNA 1 (V3SH11252-224727699, Horizon Discovery Biosciences). 48 and 72 h post-transfection, the supernatant was collected and centrifuged to separate cell debris from the viral supernatant. PEG-it solution (System Biosciences Innovation) was added to the viral supernatant, and lentivirus particles were concentrated following the manufacturer's protocol. Concentrated lentivirus aliquots (20 µl) were stored at −80 °C.

Lentiviral and retroviral transduction

For lentivirus transduction, 1 × 10^6 cells were incubated with 20 µl of concentrated lentivirus particles and TransDux Max reagents (System Biosciences Innovation) following the manufacturer's instructions. 48 h post-transduction, cells were washed and incubated in their corresponding complete media. When appropriate, 1 µg/ml puromycin (Invivogen) was added to the complete media for antibiotic selection and 250 ng/ml doxycycline (Sigma) for expression of doxycycline-inducible systems. Transduction efficiency was followed by measuring RFP expression in a CytoFLEX instrument (Beckman Coulter).

For retroviral transduction, non-tissue culture treated 12-well plates were coated overnight at 4 °C with 25 µg/ml retronectin in PBS (Takara). Plates were washed with PBS and blocked with PBS supplemented with 2% BSA for 15 min. Thawed retroviral supernatant was added at ~1 ml per well and centrifuged at 1,800 g for 1.5 h before adding 0.5 × 10^6 cells. After 48 h, transduction efficiency was checked by GFP expression in CytoFLEX instrument (Beckman Coulter). When required, transduced cells were enriched by sorting GFP-positive cells in a BD FACSAria II SORP Cell Sorter (BD Biosciences).

Lenalidomide treatment

For targeted degradation of IKAROS protein, 5 x 10^5 tumor cells were seeded in duplicate in a 24-well plate with 2 ml complete media supplemented with 0 µM, 0.1 µM, 1 µM, or 10 µM lenalidomide (Selleck Chemicals). DMSO was used as a vehicle to adjust the drug volume added. After 3, 4, or 7 days, CD19 and IKAROS levels were measured by flow cytometry.

Flow cytometry analysis

To assess CD19 and CD22 surface expression, 0.5 – 1 × 10^5 cells were washed with CSM and incubated with 100 µl antibody mix (1 µl APC anti-human CD19 (clone: HIB19, BioLegend); or 1 µl APC anti-human CD22 (clone: HIB22, BioLegend) with or without 1 µl Pacific Blue anti-human CD19 (clone: HIB19, BioLegend) in 100 µl CSM) at RT for 10 min. Cells were washed twice and resuspended in 200 µl CSM for flow analysis in CytoFLEX cytometer (Beckman Coulter).

To assess IKAROS intracellular levels, 0.5 – 1 × 10^5 cells were washed with CSM and fixed with 1.6% PFA (Electron Microscopy Sciences) in CSM for 10 min at room temperature (RT). Cells were washed twice with CSM and incubated with 1 µl Pacific Blue anti-human CD19 antibody (clone: HIB19, BioLegend) in 100 µl CSM at RT for 10 min. Cells were washed twice and permeabilized with 100 µl Methanol at 4 °C for 10 min. After three washes, cells were incubated with 1 µl Alexa Flour 647 anti-human IKAROS antibody (clone: 16B5C71, BioLegend) in 100 µl CSM at RT and 300 g for 30 min. Cells were washed twice and resuspended in 200 µl CSM for flow analysis in CytoFLEX cytometer (Beckman Coulter).

Quantification of CD19 and CD22 surface molecules on cancer lines was performed using the BD Quantibrite™ APC Fluorescence Quantitation Kit (BD Biosciences).

Flow cytometry data was analyzed using Community Cytobank software (https://community.cytobank.org/). Briefly, forward versus side scatter was used to exclude debris, while forward scatter area versus width was used for doublet exclusion. When pertinent, tumor cells were gated based on GFP (IKAROS-degron, IKAROS-degron CD19KO-FL, IK6-degron, and CD19 isoforms overexpressing cells) or RFP (IKAROS WT and KD cells) expression. Finally, CD19, CD22, and IKAROS median fluorescent intensities (MFI) were calculated in the gated population.

Generation IKAROS KD cells for ATAC-seq and RNA-seq

5 × 10^6 B-ALL cells (NALM6, REH or SUP-B15) were transduced with lentivirus expressing *IKZF1* specific (Addgene #69041) or scramble (Addgene #69040) shRNA in duplicate. 72 h post-transduction, 1 × 10^5 cells were used to check transduction efficiency, CD19 and IKAROS levels via flow cytometry analysis as described. In all cases, transduction efficiencies were over 90%.

For ATAC-seq, 50,000 cells were processed as previously reported[70]. For RNA-seq, total RNA was extracted from 3 – 5 × 10^6 cells using Rneasy kit with Dnase I treatment (QIAGEN), following manufacturer instructions. RNA libraries were performed with TruSeq stranded mRNA kit (Illumina). ATAC and RNA libraries were sequenced on the Illumina NovaSeq 6000 at MedGenome facility with paired-end 50 bp or 100 bp reads, respectively.

RNA-seq data processing

For isogenic IKAROS WT or KD B-ALL cells RNA-seq data, we sequenced an average of 42 × 10^6 reads per sample (range: 29 × 10^6 – 60 × 10^6 reads). Paired-end reads were aligned and quantified using Salmon (version 1.2.0) index against the hg38 reference genome. Gencode transcript annotations (version 37) were used for the genomic location of transcriptomic units. Reads aligning to annotated regions were summarized as counts using the R package tximport (version 1.18.0). Differential expression analyses between IKAROS WT and KD samples were performed using DESeq2 (version 1.30.1)[71]. A false discovery rate (FDR) cutoff of 0.05 was used for gene selection. Read counts were normalized using variance-stabilizing transformation (vst) built into the DESeq2 package. Gene set enrichment analysis (GSEA) was performed using the GSEA software (Broad Institute).

Raw fastq files from paired pre- and post-CD19^{neg} relapse samples from pediatric r/r B-ALL patients treated with 19.BBz[14] (n = 2), adult r/r B-ALL patients treated with blinatumomab[13] (n = 2), adult r/r LBCL patients treated with 19.28z[29,30] (n = 6), and diagnosis or relapse B-ALL patients (n = 282) from the Therapeutically Applicable Research to Generate Effective Treatments (TARGET) initiative were processed as described above.

Splicing event analysis and CD19 intron 10 retention

We used the Multivariate Analysis of Transcript Splicing[72] (rMATS; version 4.1.1) to detect and quantify alternative splicing events. Raw fastq files were aligned against the hg38 reference genome (Gencode transcript version 37) using STAR software[73] (version 2.7.8a). Bam files were sorted by coordinated and indexed with SAMtools (version 1.12). rMATS was run under default configuration with indexed bam files as input. Reads spanning exon junctions and reads that do not cross an exon boundary were used for splicing quantification. Splicing events with FDR values lower than 0.05 were called significant. Inclusion level for different splicing events: SE (skipped exon), MXE (mutually exclusive exons), A3SS (alternative 3′ splice site), A5SS (alternative 5′ splice site), and RI (retained intron) were used to perform plots and additional analysis with custom R scripts.

To re-analyze paired pre- and post-CD19^{neg} relapse B-ALL samples from Orlando et al.[11], since raw fastq files were not available, we obtained bam files with only those RNA-seq reads aligned to CD19 genes (Accession number: SRP141691). Unfortunately, these bam files had undergone Split'N'Trim step, which precludes the use of rMATS. Thus, similar to Asnani, et al.[15], we performed a visual inspection of CD19-aligned reads in the IGV browser[74] and used a custom script to quantify reads aligned to CD19 intron 2 or 10 over reads aligned to CD19 exons 2 and 3 or exons 10 and 11, respectively. In addition, out of 10 patients with matched data available, we excluded one (patient 17) from the analysis for the same reason explained in Cortés-López, et al.[27].

ATAC-seq data processing

ATAC-seq data was processed as previously described[75]. Briefly, adapters were trimmed using cutadapt, and reads were mapped using bowtie2 with a max fragment length of 2000 bp to hg38. We then filtered for non-mitochondrial reads, mapq > 20, and properly paired reads, and removed duplicates using Picard tools. De-duplicated libraries were down-sampled to 15×10^6 read pairs. Aligned, de-duplicated bam files were loaded into R using DsATAC.bam function in the ChrAccR R package. Peaks were called using macs2 with the following parameters on Tn5 insertion sites: -shift -75 −extsize 150 −nomodel −call-summits −nolambda -p 0.01 -B −SPMR. The consensus peak set across technical and biological replicates was calculated using the getConsensusPeakSet function in the ChrAccR R package. The count matrix was calculated as insertion counts across samples at consensus peak set regions using the ChrAccR regionAggregation function. DESeq2[71] was used to calculate differentially accessible peaks. Differentially accessible peaks were used to calculate motif enrichment (getMotifEnrichment function in the ChrAccR R package) using the human_pwms_v2 motif database (from the chromVARmotifs package). Adjusted p value (FDR value) was converted to -log(FDR value), and top enriched motifs were plotted by -log(FDR value). Genomic localization of consensus peak set was identified using the annotatePeak function in the ChIPseekerR package and was visualized using the IGV browser[74]. Genes harboring differentially accessible peaks on their promotor region (-3000 to + 3000 bp from transcription starting site (TSS)) were used for pathways enrichment analysis in Enrichr (https://maayanlab.cloud/Enrichr/). We used Venny 2.1 (https://bioinfogp.cnb.csic.es/tools/venny/) to define up-regulated genes that had higher accessibility to their promoter in IKAROS KD cells. Protein-protein interaction network between these genes was created with STRING[76] (https://string-db.org/), and Enrichr (https://maayanlab.cloud/Enrichr/) was used to define their lineage associations.

Viral vector construction

All DNA constructs were visualized using SnapGene software (v.7.2.1; Dotmatics), and cloning was performed using In-fusion seamless cloning (Takara).

IKAROS-degron, IK6-degron, CD19WT, CD19Int2, CD19Int10, and CD19Int2-10 sequences were ordered from IDT. IKAROS-degron and IK6-degron were cloned into a XhoI/EcoRI-digested mNeonGreen − firefly luciferase vector (graciously provided by Dr. Crystal Mackall)[77]. CD19 isoforms were inserted into SrfI/XhoI digested pMSCV-FLAG-hIKAROS-IRES-GFP vector (Addgene 74046).

19.BBz and 19.28z CAR constructs were previously cloned into the MSGV1 retroviral vector[77]. In brief, both constructs consisted of the FMC63 scFv, with 19.BBz comprising the sequence FMC63 scFv - CD8 hinge - CD8 transmembrane - 4-1BB costimulatory domain - CD3z and 19.28z comprising the sequence FMC63 scFv - CD28 hinge - CD28 transmembrane - CD28 costimulatory domain - CD3z. The 22.BBz and 19/22.BBz constructs were generated by replacing the FMC63 scFv of the 19.BBz sequence. For 22.BBz, an scFv derived from the m971 antibody was used. For 19/22.BBz, the following sequence was used: GMCSF leader sequence - FMC63 VH - G4S linker - m971 VL - Whitlow linker - m971 VH - G4S linker - FMC63 VL.

CD19 isoforms expressing tumor models

CD19 KO B-ALL (697, NALM6, NALM16, REH) cell lines were generated as described above.

After seven days, CD19^{neg} B-ALL cells were sorted using a BD FACSAria II SORP Cell Sorter (BD Biosciences). Cells were expanded for seven more days and then transduced with CD19WT-IRES-eGFP, CD19Int2-IRES-eGFP, CD19Int10-IRES-eGFP, or CD19Int2-10-IRES-eGFP expressing retrovirus. After three days, transduced cells were sorted based on GFP expression using a BD FACSAria II SORP Cell Sorter (BD Biosciences). CD19 surface expression was assessed as mentioned above.

IKAROS-degron and IK6-degron tumor models

5×10^5 REH cells were transduced with IKAROS-degron-P2A-mNeonGreen or IK6-degron-P2A-mNeonGreen expressing retrovirus. After three days, transduced cells were sorted based on GFP expression using a BD FACSAria II SORP Cell Sorter (BD Biosciences). Cells were expanded for seven days and knocked out endogenous *IKZF1*-gene using the following synthetic gRNA guides (Synthego KO kit v2): 5′-UGUCGUAGGGCGUGUCGGAC-3′, 5′-CAACAACGCCAUCAACUACC-3′, and 5′-ACCACCUCGGAACCGCCCGG-3′, and the same protocol as described above. Cells were expanded for seven more days before single-cell cloning by limiting dilution into 96-well plates. Wells containing cells were grown to dense cultures before analysis of endogenous *IKZF1* locus knockout efficiency using ICE CRISPR Analysis Tool (Synthego). Clones with 100% knockout efficiency were further characterized by IKAROS, CD19, and CD22 response to asunaprevir treatment.

To generate IKAROS-degron CD19KO-FL tumor models, endogenous *CD19* locus was knocked out in the IKAROS-degron models, as described above. After seven days, CD19^{neg} IKAROS-degron cells were sorted using a BD FACSAria II SORP Cell Sorter (BD Biosciences). Cells were expanded for seven more days and then transduced with CD19WT-IRES-eGFP. After three days, transduced cells were sorted based on CD19 expression using a BD FACSAria II SORP Cell Sorter (BD Biosciences).

Asunaprevir treatment

A total of 5 x 10^5 IKAROS-degron, IK6-degron, and IKAROS-degron CD19KO-FL tumor cells were seeded in duplicate in a 24-well plate with 2 ml complete media supplemented with 0 μM, 0.1 μM, 1 μM, or 10 μM asunaprevir (Selleck Chemicals). DMSO was used as a vehicle to adjust the drug volume added. After 3, 7, or 22 days, CD19, CD22, and IKAROS levels were measured by flow cytometry. When indicated, 1×10^6 cells were processed for CyTOF, as described above.

For expression recovery experiments, 5×10^5 IKAROS-degron or IK6-degron tumor cells were treated with 10 μM asunaprevir or DMSO

for 7 days. After that, asunaprevir-treated cells were washed, and one-half were cultured in completed media supplemented with DMSO (ASU/DMSO condition), while the other half remained in media supplemented with $10\,\mu M$ asunaprevir (ASU/ASU condition). DMSO-treated cells were maintained in media supplemented with DMSO (DMSO condition). After 9, 14, 21, and 28 days, CD19, CD22, and IKAROS levels were measured by flow cytometry.

CAR T cell production
Leukopaks from healthy donors were purchased from StemCell Technologies. Primary human T cells were purified by negative selection using the RosetteSep Human T cell Enrichment kit (StemCell Technologies) and SepMate-50 tubes. T cells were cryopreserved at 2×10^7 cells per ml in CryoStor CS10 cryopreservation medium (StemCell Technologies) until use. Isolated T-cells were activated and transduced with 19.BBz, 19.28z, 22.BBz, or 19/22.BBz CARs expressing retrovirus as described previously[77]. Unmanipulated (Mock) cells were used as control. CAR T-cell killing in vitro assays were performed on day 10 after activation.

IncuCyte tumor killing assays
IKAROS-degron and IKAROS-degron CD19KO-FL models were treated for 7 days with $10\,\mu M$ asunaprevir or DMSO. On Day 0, tumor cells were washed and set in co-cultured with mock, blinatumomab-treated (50 ng/ml, Invivogen), 19.BBz, 19.28z, 22.BBz, or 19/22.BBz CAR T cells. 5×10^4 GFP-labelled tumor cells was cocultured with 5, 1, or 0.5×10^4 CAR T cells (E:T 1:1, 1:5, 1:10) in 200 µl RPMI supplemented with 10% FBS, 10 mM HEPES, 2mM l-glutamine, $100\,U\,ml^{-1}$ penicillin and $100\,\mu g\,ml^{-1}$ streptomycin. Triplicate wells were plated in 96-well flat-bottom plates for each condition. Tumor fluorescence was monitored every 2–3 h with a ×10 objective using the IncuCyte S3 Live-Cell Analysis System (Sartorius), housed in a cell culture incubator at 37 °C and 5% $CO2$, set to take 4 images per well at each timepoint. The total integrated GFP intensity was quantified using the IncuCyte basic analyzer software feature (IncuCyte S3 v.2019B Rev2; Sartorius). Data were normalized to the first timepoint and plotted as the fold change in tumor fluorescence over time.

Statistics and reproducibility
Data were analyzed and visualized using R statistical software (http://www.r-project.org) or GraphPad Prism software. The P values were calculated with the statistical test described in the relevant figure legend. In all cases, a p-value < 0.05 was considered statistically significant. No statistical method was used to predetermine the sample size. No data were excluded from the analysis. The experiments were not randomized, and the investigators were not blinded to allocation during experiments and outcome assessment.

Reporting summary
Further information on research design is available in the Nature Portfolio Reporting Summary linked to this article.

Data availability
Mass cytometry data from clinically annotated patient samples from the CART19 cohort, CART22 cohort, and IKAROS-degron, IK6-degron, IKAROS-degron CD19KO-FL cell models are available on Community Cytobank under accession numbers 121064, 121078, and 121091, respectively. Community Cytobank is a free, cloud-based platform for analyzing, storing, and sharing flow and mass cytometry data. To access and download these files, new users need an email account to register with Community Cytobank (https://community.cytobank.org/cytobank/signup). Bulk RNA-seq and ATAC-seq data from isogenic IKAROS WT or KD B-ALL cell lines have been deposited

in NCBI Gene Expression Omnibus (GEO) and are accessible through GEO SuperSeries accession number GSE225755. Final expression matrices containing recursive substation error correction (RSEC) adjusted molecule counts per cell for single-cell CITE-seq data from PDXs are available in Mendeley data[78] [https://data.mendeley.com/datasets/x6kkjp7xyv/1]. Therapeutically Applicable Research to Generate Effective Treatments (TARGET) dataset, phs000218, used for this study, is available at https://portal.gdc.cancer.gov/projects. BAM files with RNA seq reads aligned to the CD19 gene from Orlando, E. et al.[11] can be found in the NCBI Sequence Read Archive (SRA) at SRP141691. Raw RNA-seq fastq files from Plaks, V. et al.[29] can be found under accession number PRJNA727804. Raw RNA-seq fastq files from Sotillo, E. et al.[14], Zhao, Y. et al.[13], and Sworder, B. et al.[30] were obtained after request to the corresponding authors. Raw direct RNA long-reads from one B-ALL PDX is available in the SRA, at accession number SRR14326969. Source data are provided with this paper.

Code availability
The code used for B-cell developmental classification of tumor cells has been deposited in GitHub[79]: (https://github.com/kara-davis-lab/DEVclassifier) [https://zenodo.org/records/15116054].

References
1. Childhood Leukemia — Cancer Stat Facts. https://seer.cancer.gov/statfacts/html/childleuk.html.
2. Samra, B., Jabbour, E., Ravandi, F., Kantarjian, H. & Short, N. J. Evolving therapy of adult acute lymphoblastic leukemia: state-of-the-art treatment and future directions. *J. Hematol. Oncol. 2020 131* **13**, 1–17 (2020).
3. Maude, S. L. et al. Tisagenlecleucel in children and young adults with B-cell lymphoblastic leukemia. *N. Engl. J. Med.* **378**, 439–448 (2018).
4. Shah, B. D. et al. KTE-X19 for relapsed or refractory adult B-cell acute lymphoblastic leukaemia: phase 2 results of the single-arm, open-label, multicentre ZUMA-3 study. *Lancet* **398**, 491–502 (2021).
5. Majzner, R. G. & Mackall, C. L. Clinical lessons learned from the first leg of the CAR T cell journey. *Nat. Med.* **25**, 1341–1355 (2019). *2019 259*.
6. Shah, N. N. & Fry, T. J. Mechanisms of resistance to CAR T cell therapy. *Nat. Rev. Clin. Oncol.* **16**, 372–385 (2019).
7. Mejstríková, E. et al. CD19-negative relapse of pediatric B-cell precursor acute lymphoblastic leukemia following blinatumomab treatment. *Blood Cancer J.* **7**, 659 (2017).
8. Wudhikarn, K. et al. Outcomes of relapsed B-cell acute lymphoblastic leukemia after sequential treatment with blinatumomab and inotuzumab. *Blood Adv.* **6**, 1432–1443 (2022).
9. Lamble, A. J., Kovach, A. E. & Shah, N. N. How I treat post-immunotherapy relapsed B-ALL. *Blood* https://doi.org/10.1182/blood.2024024517 (2024).
10. Fergusson, N. J., Adeel, K., Kekre, N., Atkins, H. & Hay, K. A. A systematic review and meta-analysis of CD22 CAR T-cells alone or in combination with CD19 CAR T-cells. *Front. Immunol.* **14**, (2023).
11. Orlando, E. J. et al. Genetic mechanisms of target antigen loss in CAR19 therapy of acute lymphoblastic leukemia. *Nat. Med.* **24**, 1504–1506 (2018).
12. Braig, F. et al. Resistance to anti-CD19/CD3 BiTE in acute lymphoblastic leukemia may be mediated by disrupted CD19 membrane trafficking. *Blood* **129**, 100–104 (2017).
13. Zhao, Y. et al. Tumor-intrinsic and -extrinsic determinants of response to blinatumomab in adults with B-ALL. *Blood* **137**, 471–484 (2021).
14. Sotillo, E. et al. Convergence of acquired mutations and alternative splicing of CD19 enables resistance to CART-19 Immunotherapy. *Cancer Discov.* **5**, 1282–1295 (2015).

15. Asnani, M. et al. Retention of CD19 intron 2 contributes to CART-19 resistance in leukemias with subclonal frameshift mutations in CD19. *Leuk* **34**, 1202–1207 (2019). *2019 344*.

16. Lee, B. J. et al. CD19-directed immunotherapy use in KMT2A-rearranged acute leukemia: A case report and literature review of increased lymphoid to myeloid lineage switch. *Am. J. Hematol.* **97**, E439–E443 (2022).

17. Zheng, S. et al. Modulation of CD22 protein expression in childhood leukemia by pervasive splicing aberrations: Implications for CD22-directed immunotherapies. *Blood Cancer Discov.* **3**, 103–115 (2022).

18. Libert, D. et al. Serial evaluation of CD19 surface expression in pediatric B-cell malignancies following CD19-targeted therapy. *Leuk* **34**, 3064–3069 (2020).

19. Schneider, D. et al. A tandem CD19/CD20 CAR lentiviral vector drives on-target and off-target antigen modulation in leukemia cell lines. *J. Immunother. Cancer* **5**, 42 (2017).

20. Fousek, K. et al. CAR T-cells that target acute B-lineage leukemia irrespective of CD19 expression. *Leuk* **35**, 75–89 (2020).

21. Wang, L., Zhang, Y., Anderson, E., Lamble, A. & Orentas, R. J. Bryostatin Activates CAR T-Cell Antigen-Non-Specific Killing (CTAK), and CAR-T NK-Like Killing for Pre-B ALL, While Blocking Cytolysis of a Burkitt Lymphoma Cell Line. *Front. Immunol.* **13**, 825364 (2022).

22. Aminov, S. et al. Immunotherapy-resistant acute lymphoblastic leukemia cells exhibit reduced CD19 and CD22 expression and BTK pathway dependency. *J. Clin. Invest.* **134**, e175199 (2024).

23. Agrawal, V. et al. The feasibility of additional CD19-targeted cellular therapy in relapsed/refractory B-ALL with re-emergence of CD19 antigen after prior CD19-negative relapse. *Am. J. Hematol.* **98**, E38–E40 (2023).

24. Holland, E. M. et al. Efficacy of second CAR-T (CART2) infusion limited by poor CART expansion and antigen modulation. *J. Immunother. Cancer* **10**, e004483 (2022).

25. Good, Z. et al. Single-cell developmental classification of B cell precursor acute lymphoblastic leukemia at diagnosis reveals predictors of relapse. *Nat. Med.* **24**, 474–483 (2018).

26. Krönke, J. et al. Lenalidomide causes selective degradation of IKZF1 and IKZF3 in multiple myeloma cells. *Science* **343**, 301–305 (2014).

27. Cortés-López, M. et al. High-throughput mutagenesis identifies mutations and RNA-binding proteins controlling CD19 splicing and CART-19 therapy resistance. *Nat. Commun. 2022 131* **13**, 1–17 (2022).

28. Fischer, J. et al. CD19 isoforms enabling resistance to CART-19 immunotherapy are expressed in B-ALL patients at initial diagnosis. *J. Immunother.* **40**, 187–195 (2017).

29. Plaks, V. et al. CD19 target evasion as a mechanism of relapse in large B-cell lymphoma treated with axicabtagene ciloleucel. *Blood* **138**, 1081–1085 (2021).

30. Sworder, B. J. et al. Determinants of resistance to engineered T cell therapies targeting CD19 in large B cell lymphomas. *Cancer Cell* **41**, 210–225.e5 (2023).

31. Schjerven, H. et al. Genetic analysis of Ikaros target genes and tumor suppressor function in BCR-ABL1+ pre–B ALL. *J. Exp. Med.* **214**, 793–814 (2017).

32. Chung, H. K. et al. Tunable and reversible drug control of protein production via a self-excising degron. *Nat. Chem. Biol.* **11**, 713–720 (2015).

33. Stanulla, M. et al. IKZF1 deletions in pediatric acute lymphoblastic leukemia: still a poor prognostic marker? *Blood* **135**, 252–260 (2020).

34. Churchman, M. L. et al. Efficacy of retinoids in IKZF1-mutated BCR-ABL1 acute lymphoblastic leukemia. *Cancer Cell* **28**, 343–356 (2015).

35. Majzner, R. G. et al. Tuning the antigen density requirement for CAR T-cell Activity. *Cancer Discov.* **10**, 702–723 (2020).

36. Lamble, A. et al. Preinfusion factors impacting relapse immunophenotype following CD19 CAR T cells. *Blood Adv.* https://doi.org/10.1182/BLOODADVANCES.2022007423 (2022).

37. Shah, N. N. et al. Characterization of CD22 expression in acute lymphoblastic leukemia. *Pediatr. Blood Cancer* **62**, 964–969 (2015).

38. Rosenthal, J. et al. Heterogeneity of surface CD19 and CD22 expression in B lymphoblastic leukemia. *Am. J. Hematol.* **93**, E352–E355 (2018).

39. Davis, K. L. Ikaros: master of hematopoiesis, agent of leukemia. *Ther. Adv. Hematol.* **2**, 359 (2011).

40. Rabilloud, T. et al. Single-cell profiling identifies pre-existing CD19-negative subclones in a B-ALL patient with CD19-negative relapse after CAR-T therapy. *Nat. Commun.* **12**, 1–7 (2021).

41. Bueno, C. et al. CD34+CD19−CD22+ B-cell progenitors may underlie phenotypic escape in patients treated with CD19-directed therapies. *Blood* **140**, 38–44 (2022).

42. Pillai, V. et al. CAR T-cell therapy is effective for CD19-dim B-lymphoblastic leukemia but is impacted by prior blinatumomab therapy. *Blood Adv.* **3**, 3539–3549 (2019).

43. Ruella, M. et al. Dual CD19 and CD123 targeting prevents antigen-loss relapses after CD19-directed immunotherapies. *J. Clin. Invest.* **126**, 3814–3826 (2016).

44. Fry, T. J. et al. CD22-targeted CAR T cells induce remission in B-ALL that is naive or resistant to CD19-targeted CAR immunotherapy. *Nat. Med.* **24**, 20–28 (2018).

45. Glisovic-Aplenc, T. et al. CD38 as a pan-hematologic target for chimeric antigen receptor T cells. *Blood Adv.* **7**, 4418–4430 (2023).

46. Temple, W. C. et al. Humanized nanobody anti-CD72 CAR-T cells efficiently eliminate B-cell malignancies via improved affinity for CD72 but induce persistent antigen downregulation in vivo. *Blood* **140**, 7394–7395 (2022).

47. Chen, C. et al. Single-cell multiomics reveals increased plasticity, resistant populations, and stem-cell–like blasts in KMT2A-rearranged leukemia. *Blood* **139**, 2198–2211 (2022).

48. Nagel, I. et al. Hematopoietic stem cell involvement in BCR-ABL1–positive ALL as a potential mechanism of resistance to blinatumomab therapy. *Blood* **130**, 2027–2031 (2017).

49. Jacoby, E. et al. CD19 CAR immune pressure induces B-precursor acute lymphoblastic leukaemia lineage switch exposing inherent leukaemic plasticity. *Nat. Commun.* **7**, (2016).

50. Gardner, R. et al. Acquisition of a CD19-negative myeloid phenotype allows immune escape of MLL-rearranged B-ALL from CD19 CAR-T-cell therapy. *Blood* **127**, 2406–2410 (2016).

51. Uckun, F. M., Goodman, P., Ma, H., Dibirdik, I. & Qazi, S. CD22 EXON 12 deletion as a pathogenic mechanism of human B-precursor leukemia. *Proc. Natl. Acad. Sci. USA* **107**, 16852–16857 (2010).

52. Ma, H. et al. CD22 Exon 12 deletion is a characteristic genetic defect of therapy-refractory clones in paediatric acute lymphoblastic leukaemia. *Br. J. Haematol.* **156**, 89–98 (2012).

53. Dourthe, M.-E. et al. Determinants of CD19-positive vs CD19-negative relapse after tisagenlecleucel for B-cell acute lymphoblastic leukemia. *Leuk* **1**, 1–11 (2021). *2021*.

54. Pulsipher, M. A. et al. Next-generation sequencing of minimal residual disease for predicting relapse after tisagenlecleucel in children and young adults with acute lymphoblastic leukemiaNGS-MRD and relapse risk after tisagenlecleucel for ALL. *Blood Cancer Discov.* **3**, 66–81 (2022).

55. Myers, R. M. et al. Blinatumomab nonresponse and high-disease burden are associated with inferior outcomes after CD19-CAR for B-ALL. *J. Clin. Oncol.* **40**, 932–944 (2022).

56. Mohty, B. & Mohty, M. Long-term complications and side effects after allogeneic hematopoietic stem cell transplantation: an update. *Blood Cancer J.* **1**, e16 (2011).

57. Maude, S. L. et al. Chimeric antigen receptor T cells for sustained remissions in leukemia. *N. Engl. J. Med.* **371**, 1507–1517 (2014).

58. Thudium Mueller, K. et al. Tisagenlecleucel immunogenicity in relapsed/refractory acute lymphoblastic leukemia and diffuse large B-cell lymphoma. *Blood Adv.* **5**, 4980–4991 (2021).

59. Kadauke, S. et al. Risk-adapted preemptive tocilizumab to prevent severe cytokine release syndrome after CTL019 for pediatric B-Cell acute lymphoblastic leukemia: a prospective clinical trial. *J. Clin. Oncol.* **39**, 920–930 (2021).

60. Shah, N. N. et al. CD4/CD8 T-cell selection affects chimeric antigen receptor (CAR) T-cell potency and toxicity: updated results from a phase I anti-CD22 CAR T-Cell Trial. *J. Clin. Oncol.* **38**, 1938–1950 (2020).

61. Lue, J. K. et al. Precision Targeting with EZH2 and HDAC Inhibitors in Epigenetically Dysregulated Lymphomas. *Clin. Cancer Res. J. Am. Assoc. Cancer Res.* **25**, 5271–5283 (2019).

62. Jager, A., Sarno, J. & Davis, K. L. Mass cytometry of hematopoietic cells. *Methods Mol. Biol.* **2185**, 65–76 (2021).

63. Fienberg, H. G., Simonds, E. F., Fantl, W. J., Nolan, G. P. & Bodenmiller, B. A platinum-based covalent viability reagent for single-cell mass cytometry. *Cytom. A* **81A**, 467–475 (2012).

64. Zunder, E. R. et al. Palladium-based mass tag cell barcoding with a doublet-filtering scheme and single-cell deconvolution algorithm. *Nat. Protoc.* **10**, 316–333 (2015).

65. Finck, R. et al. Normalization of mass cytometry data with bead standards. *Cytom. Part J. Int. Soc. Anal. Cytol.* **83**, 483–494 (2013).

66. Bendall, S. C. et al. Single-cell mass cytometry of differential immune and drug responses across a human hematopoietic continuum. *Science* **332**, 687–696 (2011).

67. Belkina, A. C. et al. Automated optimized parameters for T-distributed stochastic neighbor embedding improve visualization and analysis of large datasets. *Nat. Commun.* **10**, 5415 (2019).

68. Amir, E. D. et al. viSNE enables visualization of high dimensional single-cell data and reveals phenotypic heterogeneity of leukemia. *Nat. Biotechnol.* **31**, 545–552 (2013).

69. Kuleshov, M. V. et al. Enrichr: a comprehensive gene set enrichment analysis web server 2016 update. *Nucleic Acids Res.* **44**, W90–W97 (2016).

70. Buenrostro, J. D., Giresi, P. G., Zaba, L. C., Chang, H. Y. & Greenleaf, W. J. Transposition of native chromatin for fast and sensitive epigenomic profiling of open chromatin, DNA-binding proteins and nucleosome position. *Nat. Methods* **10**, 1213–1218 (2013).

71. Love, M. I., Huber, W. & Anders, S. Moderated estimation of fold change and dispersion for RNA-seq data with DESeq2. *Genome Biol.* **15**, 550 (2014).

72. Shen, S. et al. rMATS: Robust and flexible detection of differential alternative splicing from replicate RNA-Seq data. *Proc. Natl Acad. Sci. USA* **111**, E5593–E5601 (2014).

73. Dobin, A. et al. STAR: ultrafast universal RNA-seq aligner. *Bioinformatics* **29**, 15–21 (2013).

74. Robinson, J. T., Thorvaldsdóttir, H., Wenger, A. M., Zehir, A. & Mesirov, J. P. Variant review with the integrative genomics viewer. *Cancer Res.* **77**, e31-e34 (2017).

75. Baskar, R. et al. Integrating transcription-factor abundance with chromatin accessibility in human erythroid lineage commitment. *Cell Rep. Methods* **2**, 100188 (2022).

76. Szklarczyk, D. et al. The STRING database in 2021: Customizable protein-protein networks, and functional characterization of user-uploaded gene/measurement sets. *Nucleic Acids Res.* **49**, D605–D612 (2021).

77. Yamada-Hunter, S. A. et al. Engineered CD47 protects T cells for enhanced antitumour immunity. *Nature* **630**, 457–465 (2024).

78. Domizi, P. CITE-seq data from Domizi, P et al. Nat Commun. 2025. IKAROS facilitates antigen escape in the face of CD19- and CD22-targeted therapies for B-cell malignancies. Mendeley Data, V1, https://doi.org/10.17632/x6kkjp7xyv.1 (2025).

79. Pedersen, C. B. kara-davis-lab/DEVclassifier: DEVclassifier. *Zenodo* https://doi.org/10.5281/zenodo.15116054 (2025).

80. Zheng, S., Papalexi, E., Butler, A., Stephenson, W. & Satija, R. Molecular transitions in early progenitors during human cord blood hematopoiesis. *Mol. Syst. Biol.* **14**, e8041 (2018).

81. Domizi, P. (2025) https://BioRender.com/8ud04e8.

Author contributions

P.D. conceived of, designed, and led this study, designed and performed experiments, analyzed and interpreted data, generated the figures, and wrote the manuscript. J.S. and A.J.M. contributed to mass cytometry experiments and to validate the antibody panel used in these experiments. M.M. and Y.L. contributed to cell culture work, retrovirus, lentivirus generation and transduction, and flow cytometry data acquisition. K.Z.P, M.C.R., and S.A.Y-H. generated 19.BBz, 19.28z, 22.BBz, and 19/22.BBz CAR T cells and performed IncuCyte experiments. W.D.R. performed ATAC-seq libraries. B.S. and S.C.B. provided guidance for ATAC-seq experiments. R.B. contributed to ATAC-seq data analysis. B.J.S. and A.A.A. provided clinical and RNA-seq data. C.G.M., A.B.L., R.M.M, S.A.G., B.Y., H.W.W., N.N.S, and D.M.B. contributed patient samples and provided clinical data on the patients. J.S., M.C.R., R.G.M., C.L.M., D.M.B., and E.S. provided guidance and scientific input. K.L.D. conceived and designed this study, provided guidance and scientific input, interpreted data, and wrote the manuscript. All authors discussed the results and commented on the manuscript.

Competing interests

N.N.S. receives research funding from Lentigen, VOR Bio, and CARGO Therapeutics. N.N.S. has attended advisory board meetings (no honoraria) for VOR, ImmunoACT, and Sobi. S.A.G.: Research and/or clinical trial support: Novartis, Servier, Cellectis, Vertex, and Kite. Study steering committees, consulting, and/or scientific advisory boards: Novartis, Allogene, Adaptive, Cabaletta, CRISPR/Vertex, Jazz, Estrella, Eureka, Bioline Rx, and Verismo. Toxicity management patents are managed by U Penn policies. K.L.D. Research support: Jazz Pharmaceuticals, BD Biosciences, and Kite-Gilead Pharmaceuticals. Advisory Board with honoraria: Novartis. The remaining authors declare no competing interests.

Additional information

Supplementary information The online version contains supplementary material available at https://doi.org/10.1038/s41467-025-58868-2.

Correspondence and requests for materials should be addressed to Pablo Domizi or Kara L. Davis.

Peer review information *Nature Communications* thanks the anonymous reviewers for their contribution to the peer review of this work. A peer review file is available.

Reprints and permissions information is available at http://www.nature.com/reprints

Publisher's note Springer Nature remains neutral with regard to jurisdictional claims in published maps and institutional affiliations.